

1 **SIM-HOM (version 1.0): a Mechanistic Module for the**
2 **formation of highly oxygenated organic molecules from**
3 **Isoprene, Monoterpene and Sesquiterpene evaluated with**
4 **ADCHAM (version 1.0)**

5
6 Liwen Yang¹, Wei Nie^{1, 2, *}, Mikael Ehn³, Chao Yan^{2, 4}, Lubna Dada⁵, Yuliang Liu^{1, 2},
7 Pontus Roldin⁶ and Aijun Ding^{1, 2, 4}

8
9 ¹ Joint International Research Laboratory of Atmospheric and Earth System Sciences,
10 School of Atmospheric Sciences, Nanjing University, Nanjing 210023, China

11 ² National Observation and Research Station for Atmospheric Processes and
12 Environmental Change in Yangtze River Delta, Nanjing 210023, China

13 ³ Institute for Atmospheric and Earth System Research/Physics, Faculty of Science,
14 University of Helsinki, Helsinki 00014, Finland

15 ⁴ Nanjing-Helsinki Institute in Atmospheric and Earth System Sciences, Nanjing
16 University, Nanjing 210023, China

17 ⁵ Laboratory of Atmospheric Chemistry, Paul Scherrer Institute, 5232 Villigen,
18 Switzerland

19 ⁶ Division of Combustion Physics, Department of Physics, Lund University, P. O. Box
20 118SE-221 00 Lund, Sweden

21 *Correspondence: Wei Nie (niewei@nju.edu.cn)

22

23 **Abstract**

24 Biogenic volatile organic compounds (BVOCs), including isoprene, monoterpenes, and
25 sesquiterpenes, are emitted in large quantities and play a critical role in atmospheric chemistry. They
26 contribute to the formation of highly oxygenated organic molecules (HOM), which are essential for
27 new particle formation (NPF) and secondary organic aerosol (SOA) formation. However, current
28 models often oversimplify the oxidation pathways of these compounds, leading to inaccuracies in
29 predicting HOM composition and concentrations. To address this gap, we developed a mechanistic
30 module, SIM-HOM (Sesquiterpene, Isoprene and Monoterpene-derived HOM mechanism), based
31 on Master Chemical Mechanism (MCM), that explicitly incorporates autoxidation processes,
32 detailed fragmentation pathways, and RO₂-RO₂ interactions for isoprene, monoterpene, and
33 sesquiterpenes. The updated module was validated using experimental data from the Cosmics
34 Leaving OUtdoor Droplets (CLOUD) chamber, demonstrating substantial improvements in
35 simulating HOM concentrations under various conditions. Specifically, it significantly improves the
36 simulation of highly oxidized isoprene products, resolves discrepancies in monoterpene-derived
37 HOM distributions, and provides the first comprehensive parameterization of sesquiterpene
38 oxidation products. The model also captures the HOM formation under mixed precursor conditions.
39 These advancements underscore the importance of incorporating detailed molecular-level reaction
40 mechanisms into atmospheric models. Future work should focus on refining branching ratios for
41 critical reactions and investigating the influence of temperature and nitrogen oxides on HOM
42 formation, and expanding the mechanism to include additional BVOC classes. Our findings provide
43 a robust foundation for improving global atmospheric simulations of SOA formation and climate
44 interactions.

45

46 **1.introduction**

47 The continental boundary layer is profoundly influenced by biogenic volatile organic compounds
48 (BVOC) emitted by vegetation. BVOC encompass diverse compounds, including isoprene, terpenes,
49 and related species, with specific types varying by vegetation type and environmental conditions.
50 The global annual emission flux of isoprene (C₅H₈) reaches up to 594 Tg, while monoterpenes
51 (C₁₀H₁₆) are emitted approximately 95 Tg annually, sustaining mixing ratio from parts per billion
52 (ppb) levels ppb to hundreds of parts per trillion (ppt). Collectively, isoprene and monoterpenes
53 contribute about 80% of total BVOC emissions (Sindelarova et al., 2014). Sesquiterpenes, such as
54 β-caryophyllene, are emitted around 20 Tg annually and are highly reactive compounds with a C15
55 skeleton. These BVOCs react rapidly with atmospheric oxidants, including hydroxyl radicals (OH),
56 ozone (O₃), and nitrate radicals (NO₃), producing low-volatility oxygenated vapors. Among these,
57 highly oxygenated organic molecules (HOM), are particular important as they significantly
58 contribute to particle nucleation (Kirkby et al., 2016; Riccobono et al., 2014; Lehtipalo et al., 2018;
59 Liu et al., 2024), growth (Simon et al., 2020; Stolzenburg et al., 2018; Trostl et al., 2016), and
60 secondary organic aerosol (SOA) formation (Ehn et al., 2014; Nie et al., 2022; Liu et al., 2023; Sun
61 et al., 2025).

62 Peroxy radicals (RO₂) are critical intermediates in the atmospheric oxidation of BVOC and play a
63 central role in the formation of HOM. Under typical atmospheric conditions, a subset of RO₂ are
64 produced by the oxidation of monoterpenes and sesquiterpenes by O₃ or OH can undergo rapid

65 autoxidation during which internal H-shift and subsequent O₂ additions lead to the formation of
66 multifunctional, low-volatility compounds (Iyer et al., 2021; Berndt et al., 2016; Shen et al., 2022;
67 Richters et al., 2016b). The autoxidation rate is strongly sensitive to molecular structure, varying by
68 several orders of magnitude depending on functional groups, and shows significant positive
69 temperature dependence (Crouse et al., 2013; Praske et al., 2018; Moller et al., 2016; Jorgensen et
70 al., 2016; Knap and Jorgensen, 2017; Otkjaer et al., 2018). Concurrently, autoxidation competes
71 with bimolecular reactions involving NO_x, HO₂, and other RO₂ (Yang et al., 2025b). The RO₂-HO₂
72 reaction typically leads to the formation of hydroperoxides, which can contribute to HOM formation
73 or undergo further reaction. Additionally, RO₂-RO₂ can result in the formation of HOM monomers,
74 where two RO₂ react to produce two new molecules, often with one less oxygen atom than their
75 precursors. RO₂-RO₂ reactions can also form HOM dimers (Heinritzi et al., 2020; Berndt et al.,
76 2018; Ng et al., 2008), which are less volatile than HOM monomers and play a pivotal role in NPF
77 and SOA formation. The influence of nitrogen oxides (NO_x) on HOM formation is complex: NO
78 exhibits a nonlinear effect for cyclic monoterpenes, promoting HOM formation at low
79 concentrations but inhibiting it at higher levels (Nie et al., 2023); whereas for isoprene, HOM
80 formation may increase with NO (Berndt et al., 2025). NO₂ tends to suppress HOM formation by
81 consuming acyl RO₂. Therefore, an accurate depiction of HOM formation requires consideration of
82 autoxidation reactions and its competition with bimolecular RO₂ reactions, which are influenced by
83 atmospheric composition, temperature, and the structure of the oxidizing molecules. Studies on the
84 HOM formation from isoprene are limited because of its smaller molecular weight (Shen et al., 2024;
85 Zhao et al., 2021; Wang et al., 2018; Xu et al., 2021; Curtius et al., 2024; Nie et al., 2022; Liu et al.,
86 2021). It can suppress HOM formation by scavenging large RO₂ radicals formed from the oxidation
87 of other VOCs (Heinritzi et al., 2020; Mcfiggans et al., 2019).

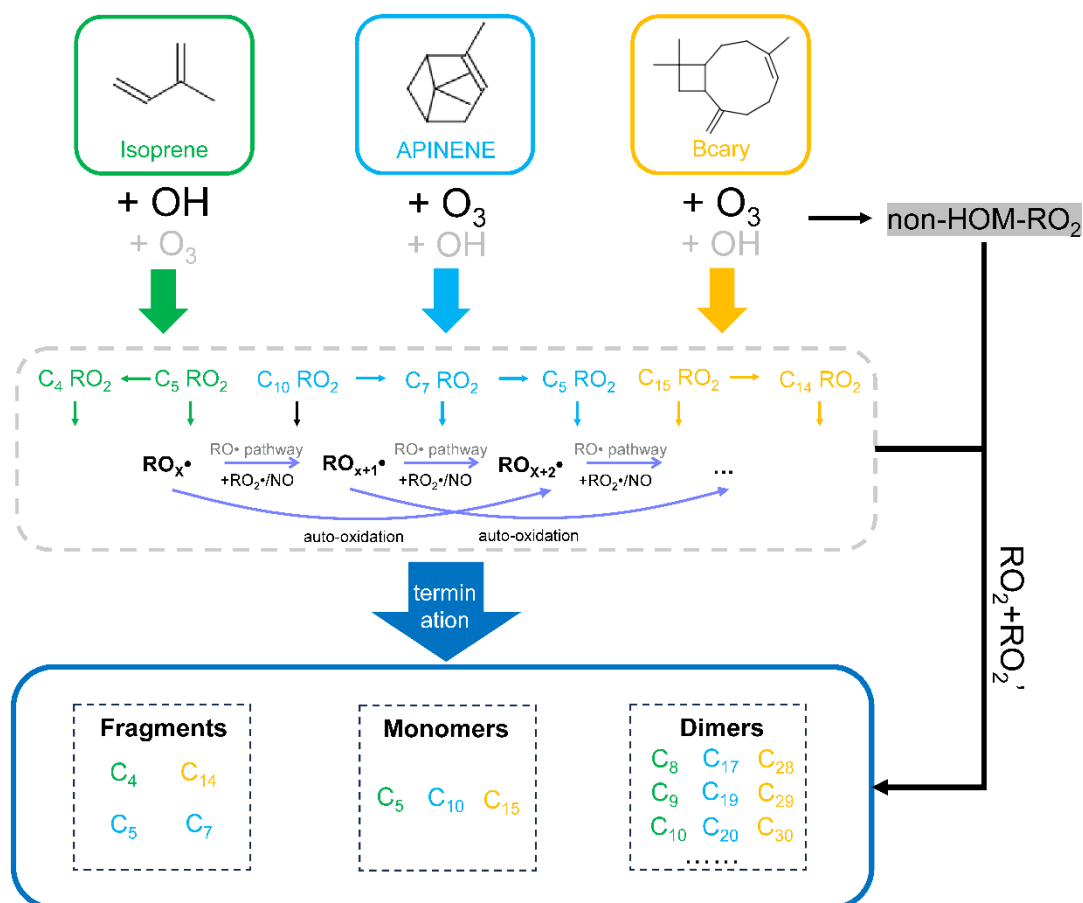
88 Insights into HOM formation mechanisms have highlighted the need to quantify their roles under
89 varying atmospheric conditions. This has been made possible by recent experimental advances, which
90 have driven the development of numerical models primarily targeting HOM mechanisms from
91 monoterpenes. Computationally efficient model like the radical two-dimensional Volatility Basic
92 Set (radical-VBS) by Schervish et al (Schervish and Donahue, 2020; Schervish et al., 2024) and
93 CRI-HOM (Weber et al., 2020) have been implemented in some large-scale models. These
94 frameworks are designed to represent the overall formation and partitioning behavior of HOM using
95 parameterized volatility distributions and oxidation pathways, rather than explicitly tracking
96 individual molecules. While grounded in mechanistic understanding, their simplified representation
97 may omit potential important aspects of chemical complexity, such as the role of specific RO₂
98 reaction pathways or the molecular identity of condensing vapors. Conversely, quasi-explicit
99 approaches, such as the method by Roldin et al (Roldin et al., 2019), provide detailed autoxidation
100 chemistry but lack comprehensive descriptions of fragmentation products. For isoprene oxidation
101 mechanisms, comprehensive models like the Master Chemical Mechanism (MCM) (Jenkin et al.,
102 2015) and Caltech isoprene mechanisms (Wennberg et al., 2018) incorporate detailed
103 representations of isoprene chemistry, consisting of hundreds of species (up to 602 in MCMv3.3.1
104 and 404 in the Caltech mechanism) and approximately 1000 reactions. While these existing models
105 emphasize radical budget, carbon cycling and SOA contributions, they often do not resolve the
106 specific HOM formation or accretion products in detail, due to their limited parameterizations.
107 Sesquiterpenes, though often omitted from current models, can exhibit HOM yields of around 2%
108 (Richters et al., 2016a; Jokinen et al., 2016) under laboratory conditions. Given their 15-carbon

109 structure, the resulting oxidation products are lower volatile than those from smaller VOCs,
110 allowing even modest HOM yields to contribute efficiently to particle-phase mass and new particle
111 growth.

112 Building upon these foundational studies, this study develops a unified and mechanistically detailed
113 mechanism, SIM-HOM (Sesquiterpene, Isoprene, and Monoterpene-derived HOM mechanism) that
114 extends HOM modeling to include not only monoterpenes and isoprene, but also sesquiterpenes, an
115 often overlooked yet potentially important contributor due to their low volatility oxidation products
116 (Dada et al., 2023). The model incorporates autoxidation and interactions among RO₂ radicals from
117 various VOCs, enabling a more comprehensive representation of HOM formation under
118 atmospherically relevant conditions. Section 2 details the model development based on existing gas-
119 phase chemical mechanisms and theoretical studies. Section 3 discusses the model validation using
120 the experiment data from Cosmics Leaving Outdoor Droplets (CLOUD) chamber, and section 4
121 summarizes this study and provides recommendations for future research.

122 **2. Mechanism development**

123 The mechanism developed in this study is primarily based on the MCM framework, chosen for its
124 comprehensive representation of organic compounds degradation in the troposphere and its ability
125 to incorporate a wide range of atmospheric chemical reactions with detailed kinetic and mechanistic
126 data. Within its framework, the gas-phase chemistry of isoprene was refined using updates from the
127 Caltech isoprene mechanism, focusing on the autoxidation pathway and HOM formation.
128 Monoterpene oxidation was addressed using modifications from the Peroxy Radical Autoxidation
129 Mechanism (PRAM), emphasizing fragmentations and ester formation as an accretion product. For
130 sesquiterpenes, a dedicated module was developed, leveraging both theoretical and experimental
131 data to represent its distinctive chemical pathways to HOM formation. Additionally, we
132 incorporated detailed interactions between different RO₂ species, including dimer formation. Figure
133 1 illustrates the primary framework of this mechanism, with specific attention to the roles of
134 unimolecular and bimolecular reactions in driving HOM production. Detailed modifications to the
135 base mechanism are described in the following sections.



136

137 Figure 1. Schematic plot showing the mechanism of HOM formation via the oxidation of isoprene,
 138 monoterpenes and sesquiterpenes in the absence of NO_x. Isoprene is primarily oxidized by OH,
 139 while monoterpenes and sesquiterpenes are primarily oxidized by O₃. A small fraction of RO₂ can
 140 undergo autoxidation (defined as p-HOM-RO₂, colored font in the figure), and the other fraction of
 141 RO₂ that cannot undergo autoxidation (defined as non-HOM-RO₂, grey-bottomed font in the figure).
 142 p-HOM-RO₂ can undergo both unimolecular and bimolecular reactions, and both can form alkoxy
 143 radicals, which can fragment or isomerize. For the dimer formation, we only consider them from
 144 RO₂-RO₂ reactions between p-HOM-RO₂ and non-HOM-RO₂.

145

146 2.1 Extension of Isoprene Oxidation Mechanism

147 In recent decades, significant advancements have been made in understanding the oxidation
 148 mechanisms of isoprene, due to its key role in atmospheric chemistry and its extremely high
 149 abundance in the atmosphere. As the most emitted BVOC globally, isoprene has been widely
 150 recognized as a significant SOA precursor, forming specific intermediates such as isoprene-
 151 epoxydiol (IEPOX) (Paulot et al., 2009; Nguyen et al., 2014) and methacryloyl peroxyoxynitrate
 152 (MPAN) (Nguyen et al., 2015), in addition to highly functionalized low-volatility compounds
 153 (Krechmer et al., 2015; D'arnbro et al., 2017; Xu et al., 2021).

154 Accurately representing the isoprene chemistry in large-scale atmospheric models is crucial but
 155 remains challenging due to the complex reaction mechanisms. MCM, through continuous updates,
 156 provides an almost complete compilation of isoprene's degradation pathways. Additionally,

157 Wennberg et al. (2018) conducted a systematic review of current knowledge on isoprene chemistry,
158 resulting in the development of the Caltech isoprene mechanism—a detailed reaction framework
159 capable of dynamically simulating the allylic and peroxy radical systems formed when isoprene
160 reacts with OH radicals (Wennberg et al., 2018). Compared to earlier mechanisms, the Caltech
161 isoprene mechanism introduces significant advancements, including the incorporation of reversible
162 O₂ addition to allyl radicals, the identification of new products from 1,6-H shifts in Z-δ-OH-peroxy
163 radicals, and a reduced yield of C₅-hydroperoxy-aldehydes (HPALD). Furthermore, it includes more
164 intramolecular H-shift processes, such as rapid peroxy-hydroperoxyl (RO₂-OOH) shifts, which
165 enhance OH recycling rates under low-nitrogen conditions. Despite these advancements, MCM
166 provides a more detailed treatment of isoprene chemistry, including more comprehensive RO₂-RO₂
167 reactions and improved photolysis processes. The photolysis rate constants in MCM are calculated
168 by integrating light flux over specific wavelengths, enabling accurate representation of photolysis
169 under varying atmospheric conditions. In contrast, the Caltech mechanism calculates photolysis
170 rates using a simplified coefficient, 'sun', which relies on sunrise and sunset times. While effective
171 for outdoor scenarios, this approach does not adequately capture the intricacies of controlled
172 laboratory illumination, making MCM the preferred mechanism for laboratory-based simulations.

173 To exploit the strengths of both mechanisms, we integrated the MCM and Caltech isoprene
174 mechanisms in our framework. This posed significant challenges due to differences in species
175 naming conventions between the two frameworks. In the MCM, compounds are named
176 systematically based on their chemical structure and assigned a unique identifier, whereas the
177 Caltech mechanism employs a naming system based on the carbon skeleton and functional group
178 positions. As a result, careful mapping of chemical species between the two mechanisms was
179 required to bridge these discrepancies (see Supplementary Information for details). This integrated
180 approach allows us to harness the complementary advantages of both mechanisms for a more robust
181 representation of isoprene chemistry.

182 Despite these improvements, the descriptions of HOM production from the oxidation of isoprene
183 remain incomplete. To address this gap, we incorporated autoxidation pathways for specific high-
184 yield RO₂ formed during isoprene oxidation, which are crucial intermediates in isoprene oxidation.
185 The key RO₂ radicals considered include those substituted with =O, -OH, and -OOH groups, which
186 originate from isoprene hydroxyperoxyl radicals (ISOPOO) and RO₂ species formed following a
187 1,6 α-hydroxy H-shift in two Z-δ-ISOPOO isomers. The rapid H-shift reactions of these high-yield
188 RO₂ radicals are critical, as they allow for the production of stable, low-volatility products under
189 typical atmospheric conditions, making them particularly potent for HOM formation.

190 For these H-shift reactions to compete effectively with bimolecular reactions involving NO, HO₂,
191 and other RO₂, unimolecular reaction rate constants need to reach approximately $\sim 10^{-2} \text{ s}^{-1}$ or higher.
192 Reported H-shift rates for these radicals cover a wide range, from 8.2×10^{-2} to $3.0 \times 10^5 \text{ s}^{-1}$ at 298
193 K (Moller et al., 2019), with hydroperoxides exhibiting notably faster rate. While the Caltech
194 isoprene mechanism assumes alkyl radicals predominantly fragment into smaller products, thus
195 limiting HOM formation, we introduced an oxygen addition pathway to alkyl radicals, as suggested
196 in (Wang et al., 2018). This modification introduces a competing reaction pathway that can produce
197 new RO₂ species, counterbalancing the dominance of fragmentation. Subsequent bimolecular
198 reactions involving these RO₂ species were implemented based on the work of (Jenkin et al., 2019).

199 Although OH oxidation overwhelmingly dominates the removal of isoprene from the atmosphere,

200 O₃ oxidation accounts for approximately 10% of isoprene's global loss (Bates and Jacob, 2019).
201 Previous models primarily focused on its contributions to the formation of methyl vinyl ketone
202 (MVK), methacrolein (MACR), CH₂OO (C1 SCI), and OH, while largely neglecting its potential
203 contribution to HOM formation. Here, we adopted a simplified approach similar to that of
204 (Schervish et al., 2024), assuming that only a small fraction of RO₂ radicals are capable of
205 undergoing autoxidation. These RO₂ radicals can subsequently participate in unimolecular or
206 bimolecular reactions, with some contributing to the HOM formation.

207 **2.2 Improvement of Monoterpene Oxidation Mechanism**

208 Our model extends the first comprehensive Peroxy Radical Autoxidation Mechanism (PRAM)
209 developed by (Roldin et al., 2019). PRAM meticulously simulates the autoxidation processes of
210 RO₂ formed from monoterpene oxidation. This mechanism has demonstrated strong agreement with
211 observed HOM concentrations, SOA mass concentrations, and NPF in boreal forest simulations.
212 However, the original PRAM only considered the HOM formation pathway via monoterpene
213 oxidation by O₃ and OH. Nie et al later expanded this mechanism by incorporating NO₃-initiated
214 oxidation pathway to the original mechanism, which mainly includes the autoxidation of
215 monoterpenes by NO₃ to form RO₂; the reaction of RO₂ with NO₃ to form RO radicals (though this
216 pathway is negligible under most environmental conditions) and bimolecular termination reactions
217 between NO₂ and specific RO₂ (e.g., acyl RO₂). (Nie et al., 2023)

218 In this study, we further optimize the key oxidation pathways of monoterpenes, with a particular
219 focus on α -pinene ozonolysis, which serves as a representative case due to its atmospheric relevance
220 and detailed mechanistic understanding. Conventional mechanisms propose that α -pinene
221 ozonolysis begins with the decomposition of the primary ozonide into a carbonyl-substituted
222 Criegee Intermediate (CI). Three isomeric forms of this CI can undergo a 1,4 H-shift to produce
223 vinyl hydroperoxide (VHP). The VHP subsequently decomposes into a vinyloxy radical, which reacts
224 with O₂ to form a RO₂ radical. However, under typical conditions, the isomerization of this RO₂
225 radical is too slow to explain the observed rapid formation of HOMs. To address this, (Iyer et al.,
226 2021) proposed a critical solution by introducing a chemically activated ring-opening reaction of
227 one of the vinyloxy radicals. This reaction leads to the rapid formation of an endoperoxide and a RO₂
228 radical with a high oxygen content (containing 8 oxygen atoms). The PRAM mechanism
229 incorporates this modification and further details the progressive increase in oxygen atoms within
230 the molecule through consecutive intramolecular RO₂ H-shifts and O₂ additions during autoxidation.
231 This autoxidation chain ultimately terminates through bimolecular reactions with NO, HO₂, or other
232 RO₂ radicals, forming a variety of products such as alkoxy radicals, closed-shell HOM monomers,
233 or dimers. Once alkoxy radicals are formed, they may undergo further transformations. For example,
234 they can isomerize into hydroxy-substituted alkyl radicals, which subsequently react with O₂ to
235 form new RO₂ species, or they may form closed-shell HOM monomers with additional carbonyl
236 groups. Alternatively, they may decompose into more volatile species. A specific example of these
237 fragment products includes the MCM-modeled RO₂ species C717O2 (an RO₂), and smaller volatile
238 species like acetone (CH₃COCH₃).

239 In our improved model, we incorporated the C7-fragment due to recent studies indicate that early-
240 formed addition products retain sufficient energy to overcome transition state barriers, leading to
241 the formation of a significant amount of alkyl radicals with an endoperoxide group (EPO). Unlike
242 the traditional view that excess energy dissipates in the next O₂ addition step, (Yang et al., 2025a)

243 demonstrated that EPO formation enables rearrangement pathways involving alkoxy radicals with
244 epoxide groups (AOE). Their study identified that cleavage reactions from these intermediates,
245 which yield acetone and C₇ products (AE-C7), are the fastest. Furthermore, the O₂ addition products
246 (RO₂) formed from AE-C7 and AE-C10 contain multiple active sites for H-shift, facilitating further
247 autoxidation. These findings provide key insights into the competition between unimolecular H-
248 shift reactions and bimolecular sinks, such as reactions with NO and HO₂. Additionally, the
249 contribution of AE-C7 and AE-C10 derivatives explains observed peaks in mass spectrometry
250 corresponding to C₇-HOMs.

251 We also incorporated RO₂-Kb β-cleavage and CH₂O loss to better represent the formation of C₁₉
252 accretion products, like C₁₉H₂₈O_x and C₁₉H₃₀O_x, as observed in experiments by Berndt et al. (Berndt
253 et al., 2018). These products are formed through RO₂ self- and cross-reactions involving CH₂O loss.
254 Furthermore, experiments that isolated OH oxidation revealed that these C₁₉ accretion products are
255 not formed through pure OH-mediated processes, but rather arise specifically from O₃-derived RO₂
256 radicals (Peräkylä et al., 2023; Kenseth et al., 2023). Our updated model explicitly accounts for
257 these distinctions, differentiating the contributions of OH- versus O₃-derived RO₂ radicals in the
258 formation of HOM accretion products.

259 **2.3 Development of Sesquiterpene Oxidation Mechanism**

260 Prior to our work, HOM formation from sesquiterpenes lacked a dedicated module in atmospheric
261 models. To address this, we developed a comprehensive framework based on the reaction pathways
262 proposed by (Richters et al., 2016b), integrating key processes derived from existing knowledge to
263 better represent the oxidation chemistry of sesquiterpenes. Given that β-caryophyllene is the only
264 sesquiterpene included in MCM, our development focuses exclusively on this compound.

265 The ozonolysis of β-caryophyllene begins with an exothermic reaction between O₃ and the double
266 bonds of sesquiterpene molecules, forming CIs with significant excess energy. These chemically
267 activated CIs can either stabilize through collisions with other molecules or undergo unimolecular
268 reactions. Stable CIs may also engage in bimolecular reactions, initiating a variety of pathways that
269 eventually lead to HOM formation. A critical step involves the isomerization of CIs into vinyl
270 hydroperoxide, which further decomposes by releasing OH radicals, producing alkyl radicals as
271 intermediates. The alkyl radicals rapidly react with O₂, forming the first generation of RO₂ radical.

272 The fate of these initial RO₂ radicals branch into several pathways. In one major pathway, the RO₂
273 radical undergoes intramolecular H-shifts followed by O₂ addition, resulting in new RO₂ radicals
274 that resemble the first-generation p-HOM-RO₂ species observed in monoterpene ozonolysis. These
275 products typically include hydroperoxide (-OOH) functionalities. Alternatively, RO₂ radicals can
276 attack the remaining double bond in the sesquiterpene structure. This process leads to the formation
277 of endoperoxides and additional alkyl radicals, which subsequently react with O₂ to form new RO₂
278 radicals, though these lack the -OOH functional group. Further reaction pathways are also possible.
279 For instance, RO₂ radicals may undergo additional intramolecular H-shifts, resulting in the
280 formation of closed-shell products along with the release of OH radicals; or the subsequent O₂
281 addition after H-shift forms a new RO₂. Another pathway involves internal RO₂ reactions with the
282 remaining double bond, which can generate cyclic R radicals. These cyclic radicals then react with
283 O₂, producing the next generation of RO₂ radicals.

284 Epoxide formation is another potential pathway, where an epoxide ring forms within the molecule,

285 followed by cleavage of the acyl alkoxy functionality and the expulsion of CO₂. This step yields
286 alkyl radicals that rapidly react with O₂ to form new RO₂ species. These RO₂ radicals can then enter
287 further autoxidation processes, involving a series of intramolecular hydrogen transfer reactions and
288 successive O₂ additions, to produce higher-generation RO₂ species.

289 By systematically integrating these reaction pathways into our model, we developed a robust
290 framework to simulate HOM formation from sesquiterpene ozonolysis. The inclusion of detailed
291 autoxidation chemistry, along with pathways involving both -OOH and non-OOH functional group
292 formation, ensures a more comprehensive representation of the sesquiterpene oxidation process and
293 its contribution to atmospheric HOM and SOA formation.

294 **2.4 RO₂ cross reactions in mixed VOC system**

295 In real atmospheric conditions, VOC mixtures produce a variety of RO₂ radicals that can react with
296 each other to form RO, closed-shell monomers, or dimers. Given the vast number of RO₂ species in
297 detailed chemical mechanisms, explicitly representing all possible cross-reactions is impractical. To
298 address this, MCM uses a simplified approach, which assumes that all RO₂ radicals interact
299 uniformly within a "RO₂ pool" at a collective rate. This is implemented using the parameter $\Sigma[\text{RO}_2]$,
300 which represents the summed concentration of all RO₂ species. Within this framework, the total rate
301 of all possible cross-reactions for a particular RO₂ radical is approximated as a pseudo-unimolecular
302 reaction with a rate coefficient of $k \times \Sigma[\text{RO}_2]$. While this simplification reduces computational
303 complexity, it overlooks the specific contributions of individual RO₂ combinations, particularly in
304 processes like dimer formation. The CRI-HOM model addresses dimerization by treating it as a
305 simplified reaction in which one RO₂ radical produces half of the total dimer product. Although
306 efficient, this approach fails to account for differences in how specific RO₂ combinations influence
307 product distributions.

308 In our improved model, we redefine dimerization as a specific bimolecular reaction between distinct
309 RO₂ species. To reduce complexity, we focus on the interactions between two key types of RO₂:
310 those capable of autoxidation and those that cannot undergo autoxidation (as represented in MCM).
311 Autoxidizable RO₂ radicals, due to their higher degree of functionalization, exhibit faster
312 dimerization rates (Berndt et al., 2018). Non-autoxidizable RO₂ radicals, which are generally
313 present at higher concentrations, can serve as reaction partners in these bimolecular reactions.
314 Reactions between two autoxidizable RO₂ are not explicitly represented, due to their extremely low
315 concentrations, which makes their contribution to dimer formation negligible. Likewise, reactions
316 between two non-autoxidizable RO₂ are not treated as explicit accretion product formation pathways
317 due to due to their products are probably not HOM. Instead, these reactions remain represented
318 within the generic RO₂ loss framework of the RO₂ pool, where they contribute to closed-shell
319 monomer formation through the pseudo-unimolecular reaction scheme. In this way, the total RO₂-
320 RO₂ reaction flux among all RO₂ species is still accounted for, while only those combinations most
321 relevant for HOM dimer formation are treated explicitly.

322 RO₂ + RO₂ rate coefficients are assigned according to the overall oxidation state and molecular size
323 of the RO₂ radicals, using the number of oxygen atoms as a proxy for the degree of functionalization.
324 This approach is consistent with the parameterization described above, where more highly
325 oxygenated and generally larger RO₂ radicals are assumed to exhibit higher reactivity in RO₂ + RO₂
326 reactions. SIM-HOM uses RO₂ + RO₂ reaction rates leading to closed-shell monomer products in

327 the range of 1×10^{-12} to 1.5×10^{-11} cm^3s^{-1} and $\text{RO}_2 + \text{RO}_2$ reactions leading to HOM dimers in the
328 range of 1×10^{-14} to 1.5×10^{-12} cm^3s^{-1} . This choice reflects the generally smaller branching fraction of
329 the accretion channel relative to the formation of monomer products. As a result, the effective
330 branching ratio toward accretion products in the model is typically on the order of $\sim 10\%$, consistent
331 with recent experimental and theoretical studies (Murphy et al., 2025; Berndt et al., 2018). Because
332 these dimers arise from explicit bimolecular reactions, the identities of these products are
333 determined by the specific pair of reacting RO_2 precursors. This approach balances computational
334 efficiency with improved accuracy, capturing the variability in RO_2 reactions and their impact on
335 product distributions, particularly in mixed VOC systems.

336 **2.5 Summary of the Model Improvements**

337 We implemented several key updates to the model, focusing on the autoxidation pathway, RO_2 - RO_2
338 interaction, fragmentation and termination processes. Together, these enhancements provide a more
339 accurate and comprehensive representation of atmospheric oxidation, enabling better simulation of
340 VOC oxidation and HOM formation:

341 (1) Expanded Autoxidation Pathways

342 We refined the autoxidation scheme for isoprene, monoterpenes, and sesquiterpenes by
343 incorporating recent experimental and theoretical advancements. Key updates include 1) High-yield
344 RO_2 autoxidation reactions for isoprene oxidation; 2) Extended formation and autoxidation
345 pathways for C_7 - RO_2 species in monoterpene oxidation; 3) Integration of new autoxidation and
346 HOM formation processes for sesquiterpenes, building on the MCM framework.

347 (2) Improved RO_2 - RO_2 Interactions

348 For permutation reactions, we maintained MCM's computationally efficient method. However, for
349 dimer formation, we moved beyond the simplified treatments used in mechanisms like CRI-HOM.
350 Our model explicitly parameterizes RO_2 - RO_2 interactions based on their VOC origins and
351 incorporates β -cleavage reactions for RO_2 from monoterpene ozonolysis during dimerization. This
352 provides a more detailed representation of dimer distributions and the behavior of mixed VOC
353 systems.

354 (3) Updated Fragmentation and Termination Pathways

355 We incorporated detailed fragmentation mechanisms for monoterpene and sesquiterpene oxidation
356 products, enabling more accurate predictions of experimental product distributions. Additionally,
357 new pathways for alkoxy radical formation and subsequent secondary RO_2 radicals were introduced,
358 improving the representation of carbon distribution among the oxidized products.

359 **3. Model Validation Based on CLOUD Experiments**

360 We validated the constructed model using experimental data from the Cosmic Leave Outdoor
361 Droplet Chamber (CLOUD) at CERN. The experiments were conducted in a 26.1 cm^3 stainless steel
362 chamber that can simulate diverse atmospheric conditions under well-controlled environments.
363 Specifically, we utilized data from the CLOUD 11 campaign conducted in the fall of 2016 (Dada et
364 al., 2023; Heinritzi et al., 2020). These experiments included oxidation of single precursors (pure
365 isoprene, α -pinene, and β -caryophyllene) and their mixtures, such as α -pinene and isoprene, or α -
366 pinene, isoprene, and β -caryophyllene. Table 1 summarizes the experimental conditions. For the
367 mixed experiments, the precursor molar ratio (sesquiterpene: monoterpene: isoprene) was set to

368 1:6:50 to mimic typical BVOC emissions in the atmosphere. Most pure α -pinene and β -
 369 caryophyllene experiments were performed under dark conditions, with OH concentration of
 370 approximately $1 \times 10^6 \text{ cm}^{-3}$, formed primarily via the BVOCs reactions with O_3 . When isoprene was
 371 added, OH is predominantly consumed by isoprene, resulting in a further lower OH concentration.
 372 To increase OH concentrations, Hamamatsu UV lamps (UVH) and UV excimer lasers (UVX) were
 373 employed. No NO_x was introduced in the experiments, effectively excluding NO_3 oxidation
 374 pathways. The CLOUD chamber is one of the most advanced reactors for replicating atmospheric
 375 conditions, ensuring that the lifetime and reaction pathways of p-HOM-RO₂ in the chamber closely
 376 resemble those in the real atmosphere. This allows p-HOM-RO₂ to undergo sufficient autoxidation.
 377 The oxidation products, i.e., oxygenated organic molecules, were measured using a nitrate chemical
 378 ionization atmospheric pressure interface time-of-flight (CI-API-ToF) mass spectrometer.

379

380 Table 1. Summary of the experimental conditions used in this study. All experiments are performed
 381 at 5°C and 40% RH.

	Exp	isoprene (ppt)	α -pinene (ppt)	Bcary (ppt)	O_3 (ppb)	UVH	UVX
isoprene system	IP-4500	4456	0	0	37.5	off	off
	IP-4500	4214	0	0	41.5	off	on
monoterpene system	MT-300	0	340	0	40.7	off	off
	MT-600	0	666	0	40.2	off	off
	MT-1200	0	1165	0	39.3	off	off
	MT-1200	0	1059	0	39.7	off	on
Sesquiterpene system	SQT-1.8	0	0	1.8	47.8	off	off
	SQT-3.3	0	0	3.3	48.5	off	off
	SQT-6.6	0	0	6.6	47.6	off	off
	SQT-6.6	0	0	6.6	48.7	on	off
Mixed system I: isoprene and monoterpene	Mix I-MT300	3962	317	0	44.9	off	off
	Mix I-MT600	3780	618	0	46.4	off	off
	Mix I-MT1200	3588	1116	0	47.6	off	off
	Mix I-MT1200	3396	1096	0	47.9	on	on
Mixed system II: isoprene, monoterpene and sesquiterpene	Mix II-Low	1471	303	3	45.6	on	off
	Mix II-Medium	2695	578	7.1	45.7	on	off
	Mix II-High	5749	1168	15.8	44.3	on	off
	Mix II-High	4578	974	15.8	44.3	on	on

382

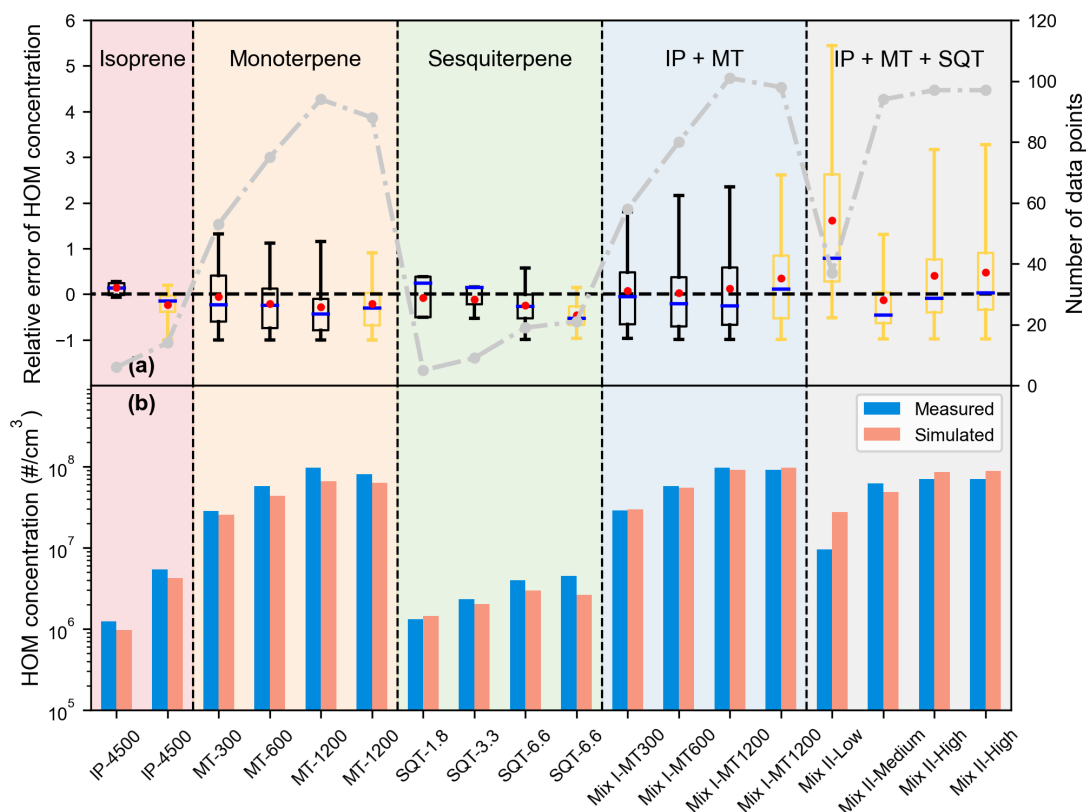
383 Our initial chemical mechanism did not account for deposition or condensation onto pre-existing
 384 aerosol surfaces. To address this limitation and isolate the effects of gas-phase chemistry, we
 385 coupled the chemical mechanism with the Aerosol Dynamics, gas- and particle-phase chemistry
 386 model for laboratory CHAMber studies (ADCHAM) (Roldin et al., 2014). ADCHAM integrates
 387 modules for aerosol dynamics, particle-phase chemistry, and a kinetic multilayer model to account

388 for diffusion-limited transport between the gas phase, particle surface, and particle bulk. Once the
389 chamber reactions reached steady-state, we simulated the HOM concentrations and compared the
390 results with experimental data. By iteratively adjusting the rate constants for autoxidation and
391 accretion product formation, we refined the chemical mechanism to achieve the best agreement with
392 experimental observations.

393 **3.1 Overall comparison**

394 To assess the model's performance under varying environmental conditions, we calculated the
395 relative error of HOM concentrations by normalizing the difference between observed and simulated
396 concentrations. Only species with concentrations exceeding $5 \times 10^4 \text{ cm}^{-3}$ (the CI-APi-ToF detection
397 limit) were considered. As shown in Figure 2a, the relative errors (defined as the difference between
398 modeled and measured HOM concentrations normalized by the measurements) are illustrated as
399 box plots. They remain close to 0 under most conditions, indicating strong agreement between
400 model and measurements. However, in the mixed system of three VOCs (IP + MT + SQT),
401 particularly at low VOC concentrations, larger discrepancies appear. This may be attributed to
402 photolysis of oxidation products by UVH lamps, which is not explicitly considered in detail, leading
403 to deviations in HOM predictions. The number of selected data points (gray dashed line) also varies
404 across different conditions, influencing error estimates.

405 Figure 2b compares the simulated and observed HOM concentrations across different VOC systems.
406 The total HOM concentration varies significantly across different precursors. The isoprene system
407 produces relatively lower HOM concentrations compared to monoterpene and sesquiterpene
408 systems, consistent with the expected differences in oxidation pathways and HOM formation
409 efficiency. The monoterpene system exhibits the highest HOM concentrations, particularly at higher
410 precursor concentrations, followed by the sesquiterpene system. In mixed systems, including the
411 isoprene-monoterpene system (Mix I) and the three-VOC mixture (Mix II), the total HOM
412 concentration increases compared to the isoprene-only system, reflecting the contribution of
413 monoterpenes and sesquiterpenes. The model successfully reproduces the general trends, capturing
414 the HOM concentrations in isoprene, monoterpene, and sesquiterpene systems, as well as in mixed
415 systems. However, overestimation is observed in some cases, particularly in low VOC concentration
416 scenarios, as discussed earlier, likely due to incomplete representation of photolysis processes.
417 Despite these minor deviations, the overall variations in HOM production across different VOC
418 regimes are well reproduced.



419

420 Figure 2. (a) Boxplots of relative errors and (b) comparison of simulated HOM and observations
 421 under different experimental conditions. From left to right, they represent pure isoprene,
 422 monoterpene, and sesquiterpene systems, the mixed system of isoprene, monoterpene, and
 423 the mixed system of the three VOCs. The specific experimental conditions are shown in Table 1.
 424 Boxplots represent medians, quartiles, and 5-95% percentiles, with red circles indicating the median,
 425 where the boxes are black in dark conditions and yellow in light conditions. The grey line indicates
 426 the number of HOM with higher concentration than the detection limit under each experimental
 427 condition. Blue and outer circles indicate observed values, pink and inner circles indicate simulated
 428 values.

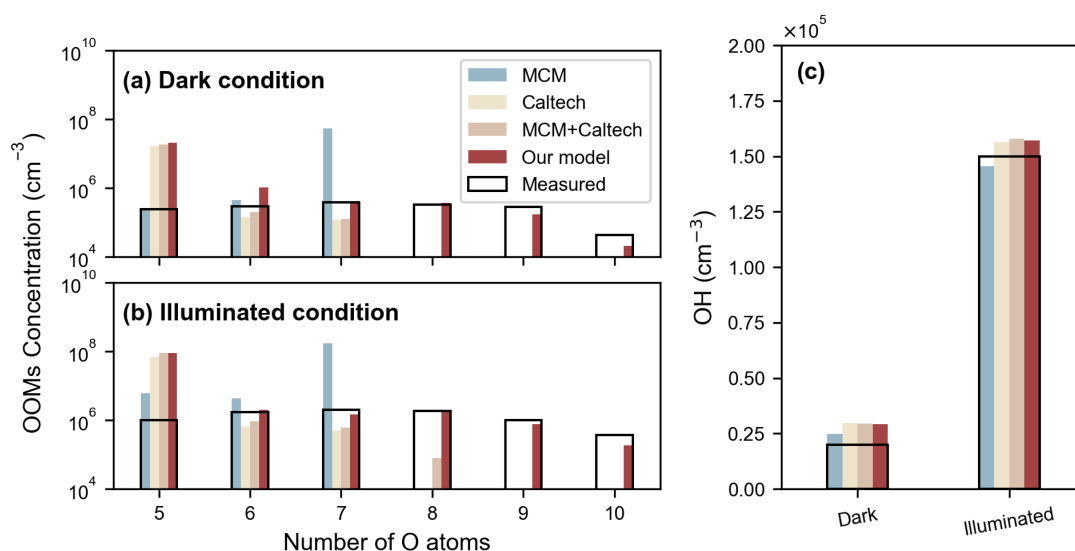
429

430 3.1 Isoprene system

431 In the pure isoprene system, the isoprene was continuously injected to maintain a concentration
 432 between 4 and 5 ppb, while O₃ was approximately 40 ppb, under both dark and illuminated
 433 conditions. We compared the simulation results from our improved module, MCM, the Caltech
 434 isoprene mechanism (Caltech), and their combination (MCM + Caltech). All models showed strong
 435 performance in predicting OH concentration (Fig. 3c).

436 Across different experimental conditions, our model exhibits significant advantages in capturing the
 437 distribution of highly oxygenated oxidation products compared to other models. For OOMs
 438 containing 5 oxygen atoms, all four models predicted concentrations notably higher than the
 439 experimental measurements (Fig. 3a and 3b), likely due to the reduced sensitivity of the NO₃-
 440 APi-ToF mass spectrometer towards OOMs with five or fewer oxygen atoms (Riva et al., 2019).
 441 For OOMs with six or seven oxygen atoms, the MCM model significantly overestimated their

442 concentrations, while the Caltech model underestimated them. In contrast, our model closely
 443 matched the measured data, indicating superior accuracy in simulating these oxidized species. More
 444 importantly, for OOMs containing eight or more oxygen atoms, our model was the only one capable
 445 of capturing their formation, underscoring its ability to accurately represent the complex pathways
 446 of HOM formation during isoprene oxidation.



447

448 Figure 3. Comparison of measured and simulated results from four models (our improved model,
 449 MCM, Caltech, and MCM + Caltech): (a) oxidation products with varying numbers of oxygen atoms
 450 under dark conditions, (b) oxidation products under illuminated conditions, and (c) OH
 451 concentration under both dark and illuminated conditions.

452 Recent studies have demonstrated that isoprene-derived highly oxygenated organic molecules (IP-
 453 HOMs) play a key role in new particle formation (NPF) in the upper troposphere (Curtius et al.,
 454 2024; Shen et al., 2024; Zha et al., 2024). Our model effectively simulates the formation of HOMs,
 455 underscoring its relevance for investigating the mechanisms of NPF and subsequent particle growth.
 456 However, the observed HOM spectrum in our chamber experiments differs from that of the
 457 atmosphere due to weak OH recycling, a consequence of the absence of NO_x and the predominantly
 458 dark or low-light experimental conditions. Atmospheric OH· levels during daytime typically remain
 459 above 10⁶ cm⁻³, even in the presence of isoprene, sustaining secondary oxidation processes. As a
 460 result, atmospheric isoprene oxidation predominantly produces C₅H₁₂O_x, C₅H₁₁NO_x and C₅H₁₀N₂O_x
 461 via second-generation OH oxidation from ISOPOOH and isoprene hydroxy nitrate (Curtius et al.,
 462 2024; Shen et al., 2024; Zha et al., 2024; Xu et al., 2021). In contrast, our experimental spectrum is
 463 dominated by C₅H₈₋₁₀O_x (Fig.S2), derived from the mono- and bimolecular reaction of RO₂ formed
 464 directly via isoprene oxidation. A comparison of C₅H₁₂O_x concentrations with other C₅ compounds
 465 (Fig.S3) further confirms that second-generation oxidation plays a minimal role in our experiments.
 466 Despite these differences, our model integrates all relevant oxidation pathways, providing a more
 467 comprehensive representation of isoprene oxidation chemistry.

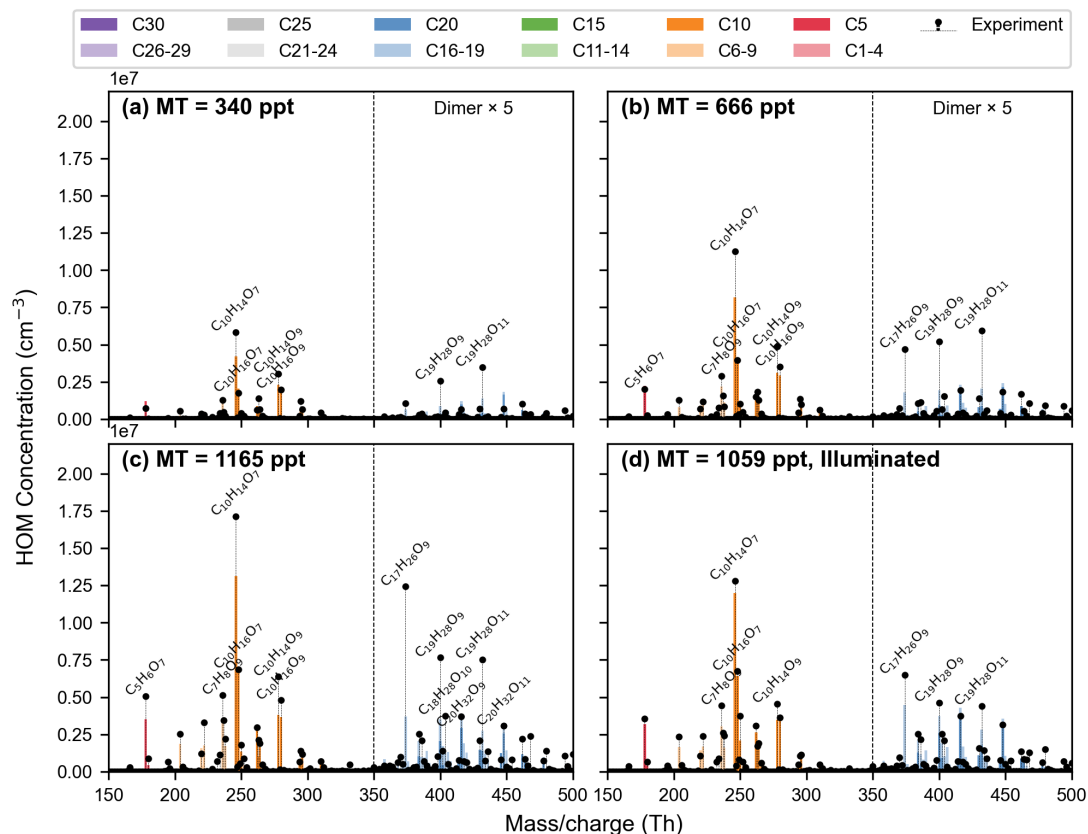
468

469 3.2 Monoterpene system

470 Fig. 4 presents the predicted oxidation products spectrum from our improved model alongside

471 experimental measurement under different conditions. A detailed comparison with the experimental
472 data demonstrates that our model achieves high accuracy in reproducing monoterpene oxidation
473 processes. In particular, it effectively captures the formation of RO₂ radicals with 10 carbon atoms
474 (C₁₀-RO₂) and accurately simulates their subsequent reaction pathways. Fragment simulation has
475 traditionally been a challenge in numerical modeling. In our improved model, we incorporated C₇
476 fragments formation by incorporating recent findings on early-stage product cleavage(Yang et al.,
477 2025a). The model successfully reproduces the isomerization of C₁₀-RO₂, leading to carbon skeleton
478 cleavage and C₇-RO₂ formation, which undergoes autoxidation and termination to produce C₇-
479 HOMs. Furthermore, C₇-RO₂ produces C₅-RO₂ through RO pathway, accurately simulating key
480 fragment products such as C₅H₆O₇, validating the model's capability in capturing essential oxidation
481 pathways.

482 Beyond accurately representing the main monomer and fragmentation product distributions, the
483 model also exhibits significant improvements in simulating dimer formation. In particular, the
484 enhanced formation of C₇-RO₂ has led to an improved prediction of C₁₇H₂₆O₉ concentration, which
485 corresponds to the most abundant dimer observed in our measurements. Additionally, the
486 incorporation of RO₂-Kb β-cleavage and CH₂O loss processes have contributed to the relatively
487 high concentrations of C₁₉H₂₈O₉ and C₁₉H₂₈O₁₁ dimers. Despite these advancements, the model still
488 slightly underestimates these dimer concentrations compared to experimental observations. Several
489 factors may contribute to this discrepancy. First, the actual yield of RO₂-Kb is higher than estimated
490 in MCM (Meder et al., 2025), leading to an underrepresentation of key dimer-forming precursors.
491 Second, RO₂-Kb cleavage products may have a higher efficiency in forming accretion products
492 compared to other RO₂, an aspect not fully accounted for in the current model. Third, additional
493 RO₂ species beyond those currently considered may undergo similar cleavage reactions,
494 contributing to dimer formation through pathways not yet incorporated (Peräkylä et al., 2023).
495 Addressing these uncertainties by refining the branching ratios and reaction rate constants of
496 dimerization pathways could help resolve these discrepancies and further improve the model's
497 predictive capabilities.



498

499 Figure 4. Comparisons between modeled and observed spectrum in α-pinene oxidation experiment
 500 with (a) 340 ppt, (b) 666 ppt, (c) 1165 ppt and (d) 1059 ppt α-pinene in (a-c) dark condition and (d)
 501 UV excimer laser (UVX) on. Mass/charge ratio is plotted in units of thomsons (Th) and it should be
 502 noted that the nitrate reagent ions has been removed from mass.

503

504 3.3 Sesquiterpene system

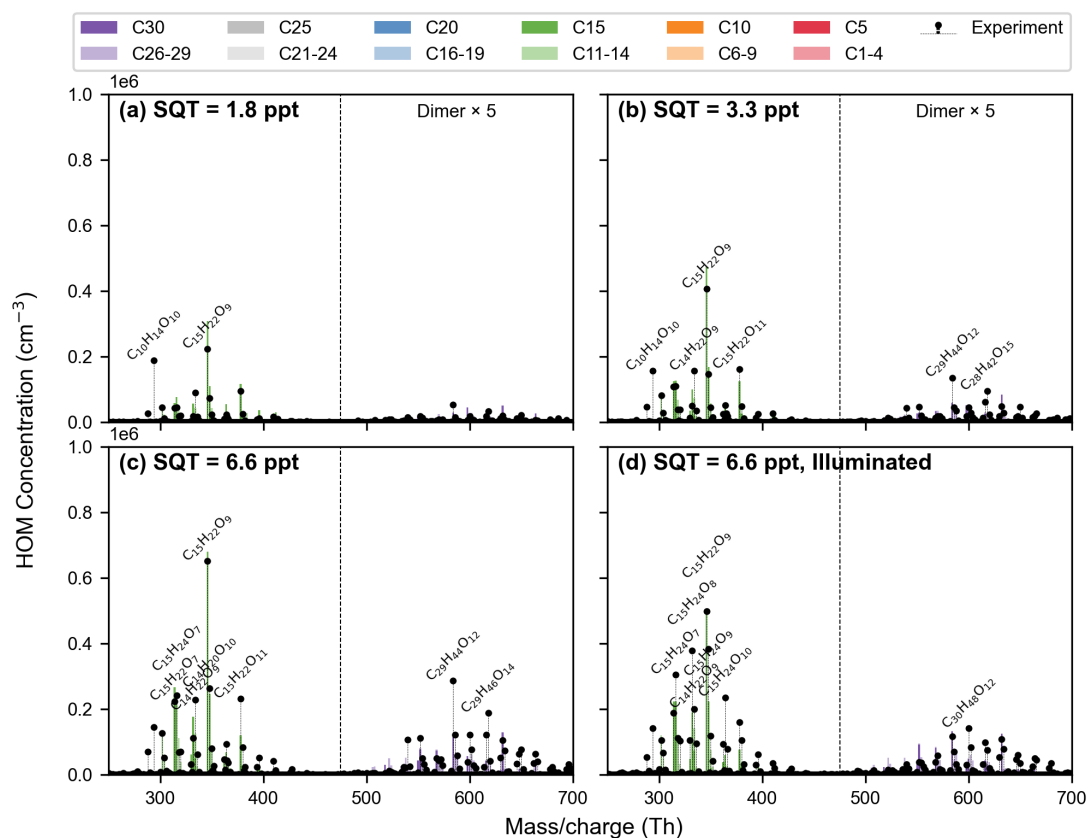
505 Fig. 5 shows that our newly developed sesquiterpene-HOM model is in strong agreement with the
 506 experimental data. During the validation process, we meticulously compared the model predictions
 507 with experimental results obtained under controlled conditions, ensuring that key chemical products
 508 - including fragmentation products, monomers, and dimers - were accurately represented. The
 509 model accurately captures the formation and transformation of these products, confirming its
 510 reliability in simulating sesquiterpene oxidation.

511 A key achievement of the model is its accurate prediction of C₁₅H₂₂O₉, the most abundant HOM
 512 molecule under these experimental conditions and a critical ELVOC contributing to NPF (Dada et
 513 al., 2023). This highlights the model's ability to capture the dominant oxidation pathways of
 514 sesquiterpenes. To comprehensively describe the reaction mechanism, we incorporated an epoxide
 515 formation step, in which CO₂ is expelled from the acyl alkoxy functional group of the intermediate,
 516 forming an alkyl radical that rapidly reacts with O₂ to form an RO₂ radical. This modification
 517 successfully explains the observed C₁₄ fragmentation product, further improving the model's
 518 accuracy in reproducing experimental spectrum. However, while the model successfully reproduces
 519 the observed peaks for most monomers and fragments, it fails to predict C₁₀H₁₄O₁₀, which is

520 detected at non-negligible concentrations in experiments. This discrepancy arises from the absence
521 of reported formation pathways for this compound, suggesting that additional reaction mechanisms
522 may need to be explored.

523 Regarding dimer formation, the model incorporates detailed RO₂ cross-reaction pathways. While
524 the model provides a reasonable overall prediction, it overestimates the concentrations of lower-
525 molecular-mass dimers while underestimating the most abundant dimers, such as C₂₉H₄₄O₁₂ and
526 C₂₉H₄₆O₁₄. This suggests that refinements in the reaction rates governing dimerization processes-
527 particular the relative contribution of RO₂-RO₂ from fragment RO₂ are necessary to achieve better
528 agreement with observations. Additionally, the inclusion of alternative dimerization channels, such
529 as those involving secondary oxidation, may be required to better represent the observed dimer
530 distribution.

531 Overall, the strong agreement between model predictions and experimental data indicates that our
532 model effectively captures the fundamental oxidation mechanism governing sesquiterpene-derived
533 HOM formation. By incorporating detailed reaction pathways and refining key parameters, the
534 model not only reproduces observed concentration but also provides mechanistic insights into HOM
535 formation. These advancements establish our sesquiterpene-HOM module as a valuable tool for
536 simulating complex chemistry under atmospheric conditions.

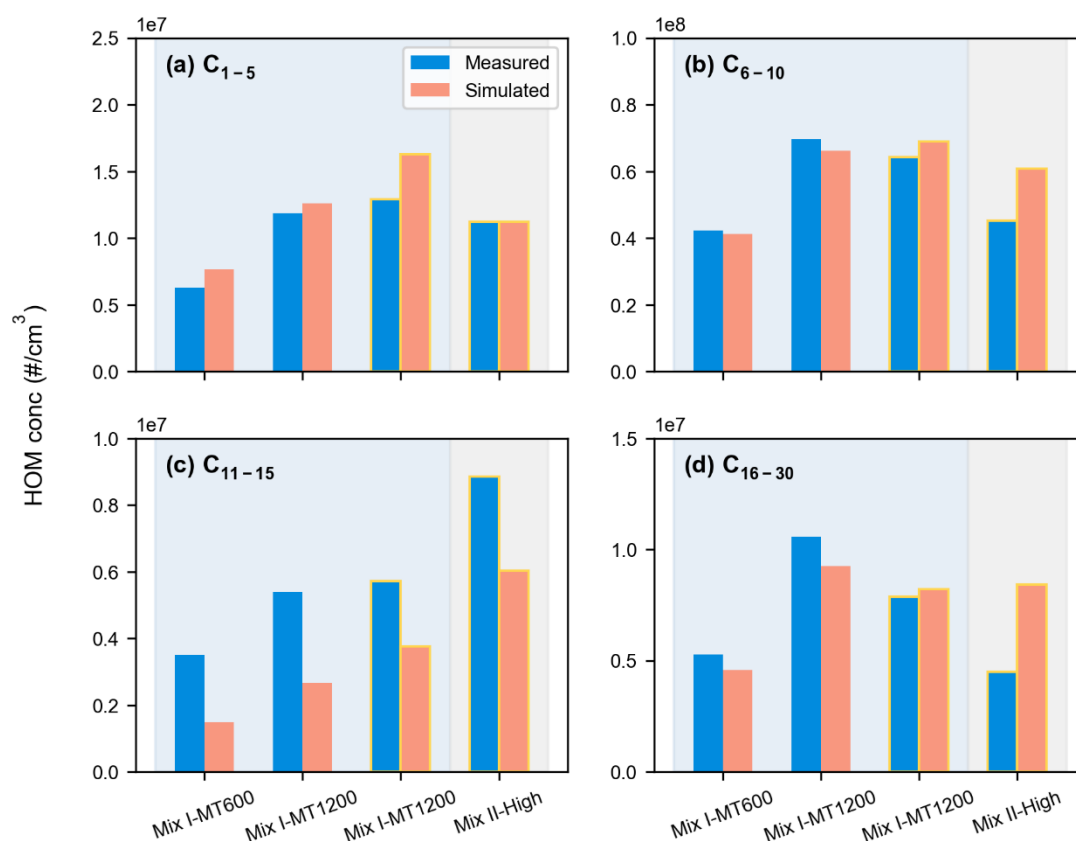


537

538 Figure 5. Comparisons between modeled and observed spectrum in β -caryophyllene oxidation
539 experiment with (a) 1.8 ppt, (b) 3.3 ppt and (c-d) 6.6 ppt β -caryophyllene in (a-c) dark condition
540 and (d) Hamamatsu UV lamps (UVH) on. Mass/charge ratio is plotted in units of thomsons (Th)
541 and it should be noted that the nitrate reagent ions has been removed from mass.

542 3.4 Mixed system

543 In this section, we compared the observed and simulated HOM concentrations in mixed systems
 544 under various conditions, including different VOC combinations, changes in VOC concentrations
 545 and the introduction of UV light (see Fig.S4 and Fig.S5). Across all cases, the simulations overall
 546 matched the observed HOM distributions, accurately reproducing key peaks and maintaining the
 547 expected carbon number distributions. Additionally, we analyzed the variation in HOM
 548 concentrations with different carbon numbers for four representative mixing conditions: (1) a
 549 mixture of isoprene and monoterpenes (Mix I-MT600), (2) an increased monoterpene concentration
 550 (Mix I-MT1200), (3) the introduction of UV light (Mix I-MT1200, Illuminated), and (4) the
 551 subsequent addition of sesquiterpenes (Mix II-High, Illuminated).



552

553 Figure 6. Experimental and simulated HOM concentration for different carbon numbers in four
 554 different mix systems (Mix I-MT600: 600 ppt α -pinene + 4 ppb isoprene; Mix I-MT1200: 1200
 555 ppt α -pinene + 4 ppb isoprene; Mix I-MT1200: 1200 ppt α -pinene + 4 ppb isoprene, illuminated;
 556 Mix II-High: 1200 ppt α -pinene + 6 ppb isoprene + 16 ppt β -caryophyllene, illuminated,
 557 respectively.). Blue bars indicate observed values and pink bars indicate simulated values, where no
 558 edge color indicates dark conditions and yellow edge color indicates light conditions. The light blue
 559 background indicates the mixed system I of isoprene and monoterpenes, and the grey background
 560 indicates the mixed system II of the three VOCs. The specific experimental conditions are shown in
 561 Table 1.

562

563 In the initial isoprene–monoterpene mixture, oxidation led to a diverse range of HOMs from both

564 C₅- and C₁₀-RO₂ pathways (Fig. S4a). Increasing the monoterpene concentration enhanced HOM
565 formation, particularly for monoterpene-derived species, like C₆₋₁₀- and C₁₆₋₂₀-HOMs (from Mix I-
566 MT600 to Mix I-MT1200, Fig.6b and 6d). The introduction of UV light shifted the HOM
567 distribution by promoting isoprene oxidation, leading to an increase in C₁₋₅- and C₁₁₋₁₅-HOMs (from
568 Mix I-MT1200 to Mix I-MT1200, illuminated, Fig.6a and 6c) while reducing monoterpene-derived
569 termination products, in particular dimers with more than 15 carbon atoms. However, the model
570 underestimated C₁₁₋₁₅-HOM concentrations, likely due to an underrepresentation of cross-reaction
571 between isoprene-derived and monoterpene-derived RO₂. The addition of sesquiterpenes further
572 altered HOM distribution, notably increasing C₁₁₋₁₅-HOM (Fig.6c), suggesting sesquiterpenes
573 exhibit a higher propensity for autoxidation and further amplifying these product channels. However,
574 the significant decrease in C₁₆₋₃₀-HOM concentration observed in three-VOC mixture, which was
575 not reflected in the simulations (Fig.6d), could be attributed to the overestimated rate of dimer
576 formation involving sesquiterpenes. This shift was likely driven by the competitive consumption of
577 available RO₂ radicals, which are reflected in both observations and models. Our model's ability to
578 simulate key features—such as the redistribution of HOM classes due to competitive RO₂
579 chemistry—demonstrates its robustness in simulating the oxidation of complex VOC mixtures. This
580 agreement highlights the model's capability to provide mechanistic insights into HOM formation
581 under varied atmospheric conditions.

582 **4. Conclusion**

583 In this study, we developed a novel and comprehensive mechanism, SIM-HOM (Sesquiterpene,
584 Isoprene, and Monoterpene-derived HOM mechanism), for simulating the HOM formation from
585 isoprene, monoterpenes, and sesquiterpenes. This mechanism incorporates intricate processes such
586 as autoxidation and interactions among RO₂ radicals derived from various BVOC, providing a more
587 nuanced understanding of the chemical transformations leading to HOM formation. The mechanism
588 was rigorously optimized and validated using experimental data obtained from the CLOUD chamber,
589 thereby demonstrating its robust capability to accurately reproduce the observed concentrations of
590 HOMs under various conditions. From an atmospheric perspective, this model is particularly
591 valuable for understanding NPF and SOA formation. Recent studies have highlighted the nucleating
592 potential of isoprene-derived HOMs, a process that our mechanism captures effectively. In fact, our
593 model is the only one capable of simulating isoprene HOMs, which represents a crucial
594 advancement in understanding NPF. Another key innovation of our work is the refinement of the
595 monoterpene oxidation mechanism, which was already recognized as crucial in previous models,
596 but is now further optimized to improve its representation of HOM formation. Furthermore, the
597 inclusion of sesquiterpene-derived HOMs, which are key contributors to NPF as shown in recent
598 literature, makes this model the first to integrate these VOCs-derived HOM in a comprehensive
599 framework. Importantly, the improved HOM parameterization introduced here bridges the gap
600 between detailed gas-phase chemistry and aerosol-phase processes. It is increasingly recognized
601 that not all HOM contribute equally to SOA formation: some exhibit low volatility and can
602 irreversibly condense onto particles, while others are semi-volatile and may evaporate on short
603 timescales. Our framework captures these differences by resolving HOM at a near-molecular level,
604 thereby improving predictions of both short-lived SOA and more stable aerosol mass that influences
605 air quality and climate-relevant properties, such as cloud formation. Overall, our model significantly
606 enhances the ability of atmospheric simulations to link specific oxidation pathways to aerosol
607 formation outcomes, thereby offering a more mechanistic foundation for understanding and

608 predicting NPF and SOA formation across diverse environments.

609 However, several limitations need to be addressed. First, the model does not yet fully incorporate
610 NO_x-related pathways. Given the significant role of NO_x in HOM formation, especially in polluted
611 environments, refining these pathways is critical for improving predictions under high-NO_x
612 conditions. In particular, the potential contribution of NO₃-initiated oxidation to HOM formation is
613 not yet represented in the current version of the model. Recent studies suggest that the importance
614 of NO₃ chemistry is strongly compound-dependent. For example, laboratory measurements indicate
615 that HOM yields from isoprene + NO₃ reactions (~1.2%) (Zhao et al., 2021) are substantially higher
616 than those from isoprene oxidation by O₃ or OH (Jokinen et al., 2015), implying that NO₃ chemistry
617 may represent an important nighttime source of HOMs from isoprene. For larger BVOCs such as
618 sesquiterpenes, their multiple double bonds and high reactivity may also favor rapid autoxidation
619 following NO₃ addition, potentially leading to efficient HOM formation. In contrast, monoterpenes
620 already exhibit substantial HOM production through O₃ and OH oxidation (Ehn et al., 2014; Kirkby
621 et al., 2016), suggesting that NO₃ chemistry may play a less dominant role, although it could still
622 contribute under certain nocturnal conditions. Due to the limited availability of systematic
623 experimental data, particularly for isoprene and sesquiterpene NO₃ oxidation, these pathways are
624 not yet explicitly included in the present mechanism and represent an important direction for future
625 model development.

626 Additionally, the model does not yet incorporate photolysis reactions comprehensively, which can
627 significantly alter the fate of HOMs and oxidation products under experimental conditions, such as
628 utilizing UV lamps in the CLOUD chamber. Moreover, in the isoprene mechanism,
629 multigenerational oxidation plays a crucial role, but its contribution to HOMs in laboratory
630 experiments is likely lower than observed in the atmosphere. Another limitation lies in the branching
631 ratios of key reactions, which govern the probability of different chemical pathways during
632 autoxidation. Refining these ratios will be essential for the model's predictive capability. Expanding
633 the mechanism to include a wider range of VOCs and their oxidation products, and considering the
634 influence of environmental factors like temperature and atmospheric composition, will further
635 improve its applicability under diverse conditions.

636 Looking forward, an important challenge lies in simplifying the mechanism for integration into
637 computationally efficient atmospheric models, such as global or regional climate models. While our
638 mechanism provides valuable insights into the chemical processes of HOM formation, its
639 complexity poses a challenge for large-scale simulations. Developing simplified parameterizations
640 that retain the key atmospheric processes while reducing computational costs will be a key step in
641 facilitating its integration into broader atmospheric models for climate and air quality forecasting.
642 In conclusion, this model represents a significant advancement in understanding of HOM formation
643 and its role in atmospheric processes. However, further improvements, especially in refining NO_x
644 interactions, photolysis processes and constraining multigenerational oxidation in the isoprene
645 system, are necessary to fully realize its potential. And efforts to simplify the mechanism for large-
646 scale models, will be essential for broader implementation in atmospheric science and policy.

647

648 **Code and data availability.**

649 The ADCHAM (version 1.0) code coupled with SIM-HOM (version 1.0) mechanism used in this

650 study is publicly available at <https://doi.org/10.5281/zenodo.19047874> (Yang et al., 2026). The
651 repository also includes the model output generated in this study.

652

653 **Author contributions.**

654 W.N. designed the study. L.Y performed model simulations and analyzed the data. W.N., M.E, C.Y.,
655 L.D, Y.L., P.R. and A.D. are acknowledged for valuable discussions. L.Y. and W.N wrote the
656 manuscript. M.E. and L.D. contributed to editing the manuscript.

657

658 **Competing interests.**

659 The authors declare that they have no conflict of interest.

660

661 **Acknowledgements.**

662 We thank CERN-CLOUD for providing experimental data, and the High-Performance Computing
663 Center of Nanjing University for providing computing resources. This work was supported by the
664 National Natural Science Foundation of China (NSFC) project (42220104006), the Jiangsu Province
665 Outstanding Youth Fund (BK20240067), the Natural Science Foundation of Jiangsu Province
666 (BK20230773), the Jiangsu Provincial Collaborative Innovation Center of Climate Change, and the
667 Fundamental Research Funds for the Central Universities.

668

669 **Reference:**

670 Bates, K. H. and Jacob, D. J.: A new model mechanism for atmospheric oxidation of isoprene: global
671 effects on oxidants, nitrogen oxides, organic products, and secondary organic aerosol, *Atmos. Chem.*
672 *Phys.*, 19, 9613-9640, 10.5194/acp-19-9613-2019, 2019.

673 Berndt, T., Hoffmann, E. H., Tilgner, A., and Herrmann, H.: Highly oxidized products from the
674 atmospheric reaction of hydroxyl radicals with isoprene, *Nat. Commun.*, 16, 12, 10.1038/s41467-025-
675 57336-1, 2025.

676 Berndt, T., Mender, B., Scholz, W., Fischer, L., Herrmann, H., Kulmala, M., and Hansel, A.: Accretion
677 Product Formation from Ozonolysis and OH Radical Reaction of α -Pinene: Mechanistic Insight and the
678 Influence of Isoprene and Ethylene, *Environmental Science & Technology*, 52, 11069-11077,
679 10.1021/acs.est.8b02210, 2018.

680 Berndt, T., Richters, S., Jokinen, T., Hyttinen, N., Kurten, T., Otkjaer, R. V., Kjaergaard, H. G., Stratmann,
681 F., Herrmann, H., Sipila, M., Kulmala, M., and Ehn, M.: Hydroxyl radical-induced formation of highly
682 oxidized organic compounds, *Nat. Commun.*, 7, 10.1038/ncomms13677, 2016.

683 Crouse, J. D., Nielsen, L. B., Jorgensen, S., Kjaergaard, H. G., and Wennberg, P. O.: Autoxidation of
684 Organic Compounds in the Atmosphere, *J. Phys. Chem. Lett.*, 4, 3513-3520, 10.1021/jz4019207, 2013.

685 Curtius, J., Heinritzi, M., Beck, L. J., Pöhlker, M. L., Tripathi, N., Krumm, B. E., Holzbeck, P.,
686 Nussbaumer, C. M., Pardo, L. H., Klimach, T., Barmounis, K., Andersen, S. T., Bardakov, R., Bohn, B.,
687 Cecchini, M. A., Chaboureau, J. P., Dauhut, T., Dienhart, D., Dörich, R., Edtbauer, A., Giez, A., Hartmann,
688 A., Holanda, B. A., Joppe, P., Kaiser, K., Keber, T., Klebach, H., Krüger, O. O., Kürten, A., Mallaun, C.,
689 Marno, D., Martinez, M., Monteiro, C., Nelson, C., Ort, L., Raj, S. S., Richter, S., Ringsdorf, A., Rocha,
690 F., Simon, M., Sreekumar, S., Tsokankunku, A., Unfer, G. R., Valenti, I. D., Wang, N. J., Zahn, A.,
691 Zauner-Wieczorek, M., Albrecht, R. I., Andreae, M. O., Artaxo, P., Crowley, J. N., Fischer, H., Harder,

692 H., Herdies, D. L., Machado, L. A. T., Pöhlker, C., Pöschl, U., Possner, A., Pozzer, A., Schneider, J.,
693 Williams, J., and Lelieveld, J.: Isoprene nitrates drive new particle formation in Amazon's upper
694 troposphere, *Nature*, 636, 23, 10.1038/s41586-024-08192-4, 2024.

695 D'Arnbro, E. L., Moller, K. H., Lopez-Hilfiker, F. D., Schobesberger, S., Liu, J. M., Shilling, J. E., Lee,
696 B., Kjaergaard, H. G., and Thornton, J. A.: Isomerization of Second-Generation Isoprene Peroxy Radicals:
697 Epoxide Formation and Implications for Secondary Organic Aerosol Yields, *Environ. Sci. Technol.*, 51,
698 4978-4987, 10.1021/acs.est.7b00460, 2017.

699 Dada, L., Stolzenburg, D., Simon, M., Fischer, L., Heinritzi, M., Wang, M. Y., Xiao, M., Vogel, A. L.,
700 Ahonen, L., Amorim, A., Baalbaki, R., Baccarini, A., Baltensperger, U., Bianchi, F., Daellenbach, K. R.,
701 DeVivo, J., Dias, A., Dommen, J., Duplissy, J., Finkenzeller, H., Hansel, A., He, X. C., Hofbauer, V.,
702 Hoyle, C. R., Kangasluoma, J., Kim, C., Kürten, A., Kvashnin, A., Mauldin, R., Makhmutov, V., Marten,
703 R., Mentler, B., Nie, W., Petäjä, T., Quéléver, L. L. J., Saathoff, H., Tauber, C., Tome, A., Molteni, U.,
704 Volkamer, R., Wagner, R., Wagner, A. C., Wimmer, D., Winkler, P. M., Yan, C., Zha, Q. Z., Rissanen, M.,
705 Gordon, H., Curtius, J., Worsnop, D. R., Lehtipalo, K., Donahue, N. M., Kirkby, J., El Haddad, I., and
706 Kulmala, M.: Role of sesquiterpenes in biogenic new particle formation, *Science Advances*, 9,
707 10.1126/sciadv.adi5297, 2023.

708 Ehn, M., Thornton, J. A., Kleist, E., Sipila, M., Junninen, H., Pullinen, I., Springer, M., Rubach, F.,
709 Tillmann, R., Lee, B., Lopez-Hilfiker, F., Andres, S., Acir, I. H., Rissanen, M., Jokinen, T., Schobesberger,
710 S., Kangasluoma, J., Kontkanen, J., Nieminen, T., Kurten, T., Nielsen, L. B., Jorgensen, S., Kjaergaard,
711 H. G., Canagaratna, M., Dal Maso, M., Berndt, T., Petaja, T., Wahner, A., Kerminen, V. M., Kulmala, M.,
712 Worsnop, D. R., Wildt, J., and Mentel, T. F.: A large source of low-volatility secondary organic aerosol,
713 *Nature*, 506, 476-479, 10.1038/nature13032, 2014.

714 Heinritzi, M., Dada, L., Simon, M., Stolzenburg, D., Wagner, A. C., Fischer, L., Ahonen, L. R.,
715 Amanatidis, S., Baalbaki, R., Baccarini, A., Bauer, P. S., Baumgartner, B., Bianchi, F., Brilke, S., Chen,
716 D. X., Chiu, R., Dias, A., Dommen, J., Duplissy, J., Finkenzeller, H., Frege, C., Fuchs, C., Garmash, O.,
717 Gordon, H., Granzin, M., El Haddad, I., He, X. C., Helm, J., Hofbauer, V., Hoyle, C. R., Kangasluoma,
718 J., Keber, T., Kim, C., Kürten, A., Lamkaddam, H., Laurila, T. M., Lampilahti, J., Lee, C. P., Lehtipalo,
719 K., Leiminger, M., Mai, H. J., Makhmutov, V., Manninen, H. E., Marten, R., Mathot, S., Mauldin, R. L.,
720 Mentler, B., Molteni, U., Müller, T., Nie, W., Nieminen, T., Onnela, A., Partoll, E., Passananti, M., Petäjä,
721 T., Pfeifer, J., Pospisilova, V., Quéléver, L. L. J., Rissanen, M. P., Rose, C., Schobesberger, S., Scholz,
722 W., Scholze, K., Sipilä, M., Steiner, G., Stozhkov, Y., Tauber, C., Tham, Y. J., Vazquez-Pufleau, M.,
723 Virtanen, A., Vogel, A. L., Volkamer, R., Wagner, R., Wang, M. Y., Weitz, L., Wimmer, D., Xiao, M., Yan,
724 C., Ye, P. L., Zha, Q. Z., Zhou, X. Q., Amorim, A., Baltensperger, U., Hansel, A., Kulmala, M., Tomé,
725 A., Winkler, P. M., Worsnop, D. R., Donahue, N. M., Kirkby, J., and Curtius, J.: Molecular understanding
726 of the suppression of new-particle formation by isoprene, *Atmospheric Chemistry and Physics*, 20,
727 11809-11821, 10.5194/acp-20-11809-2020, 2020.

728 Iyer, S., Rissanen, M. P., Valiev, R., Barua, S., Krechmer, J. E., Thornton, J., Ehn, M., and Kurtén, T.:
729 Molecular mechanism for rapid autoxidation in α -pinene ozonolysis, *Nat. Commun.*, 12, 6,
730 10.1038/s41467-021-21172-w, 2021.

731 Jenkin, M. E., Young, J. C., and Rickard, A. R.: The MCM v3.3.1 degradation scheme for isoprene,
732 *Atmospheric Chemistry and Physics*, 15, 11433-11459, 10.5194/acp-15-11433-2015, 2015.

733 Jenkin, M. E., Valorso, R., Aumont, B., and Rickard, A. R.: Estimation of rate coefficients and branching
734 ratios for reactions of organic peroxy radicals for use in automated mechanism construction, *Atmospheric*

735 Chemistry and Physics, 19, 7691-7717, 10.5194/acp-19-7691-2019, 2019.

736 Jokinen, T., Kausiala, O., Garmash, O., Peräkylä, O., Junninen, H., Schobesberger, S., Yan, C., Sipilä,
737 M., and Rissanen, M. P.: Production of highly oxidized organic compounds from ozonolysis of β -
738 caryophyllene: laboratory and field measurements, *Boreal Environment Research*, 21, 262-273, 2016.

739 Jokinen, T., Berndt, T., Makkonen, R., Kerminen, V. M., Junninen, H., Paasonen, P., Stratmann, F.,
740 Herrmann, H., Guenther, A. B., Worsnop, D. R., Kulmala, M., Ehn, M., and Sipilä, M.: Production of
741 extremely low volatile organic compounds from biogenic emissions: Measured yields and atmospheric
742 implications, *Proc. Natl. Acad. Sci. U. S. A.*, 112, 7123-7128, 10.1073/pnas.1423977112, 2015.

743 Jorgensen, S., Knap, H. C., Otkjaer, R. V., Jensen, A. M., Kjeldsen, M. L. H., Wennberg, P. O., and
744 Kjaergaard, H. G.: Rapid Hydrogen Shift Scrambling in Hydroperoxy-Substituted Organic Peroxy
745 Radicals, *J. Phys. Chem. A*, 120, 266-275, 10.1021/acs.jpca.5b06768, 2016.

746 Kenseth, C. M., Hafeman, N. J., Rezgui, S. P., Chen, J., Huang, Y. L., Dalleska, N. F., Kjaergaard, H. G.,
747 Stoltz, B. M., Seinfeld, J. H., and Wennberg, P. O.: Particle-phase accretion forms dimer esters in pinene
748 secondary organic aerosol, *Science*, 382, 787-792, 10.1126/science.adi0857, 2023.

749 Kirkby, J., Duplissy, J., Sengupta, K., Frege, C., Gordon, H., Williamson, C., Heinritzi, M., Simon, M.,
750 Yan, C., Almeida, J., Trostl, J., Nieminen, T., Ortega, I. K., Wagner, R., Adamov, A., Amorim, A.,
751 Bernhammer, A. K., Bianchi, F., Breitenlechner, M., Brilke, S., Chen, X. M., Craven, J., Dias, A., Ehrhart,
752 S., Flagan, R. C., Franchin, A., Fuchs, C., Guida, R., Hakala, J., Hoyle, C. R., Jokinen, T., Junninen, H.,
753 Kangasluoma, J., Kim, J., Krapf, M., Kurten, A., Laaksonen, A., Lehtipalo, K., Makhmutov, V., Mathot,
754 S., Molteni, U., Onnela, A., Perakyla, O., Piel, F., Petaja, T., Praplan, A. P., Pringle, K., Rap, A., Richards,
755 N. A. D., Riipinen, I., Rissanen, M. P., Rondo, L., Sarnela, N., Schobesberger, S., Scott, C. E., Seinfeld,
756 J. H., Sipilä, M., Steiner, G., Stozhkov, Y., Stratmann, F., Tome, A., Virtanen, A., Vogel, A. L., Wagner,
757 A. C., Wagner, P. E., Weingartner, E., Wimmer, D., Winkler, P. M., Ye, P. L., Zhang, X., Hansel, A.,
758 Dommen, J., Donahue, N. M., Worsnop, D. R., Baltensperger, U., Kulmala, M., Carslaw, K. S., and
759 Curtius, J.: Ion-induced nucleation of pure biogenic particles, *Nature*, 533, 521-526,
760 10.1038/nature17953, 2016.

761 Knap, H. C. and Jorgensen, S.: Rapid Hydrogen Shift Reactions in Acyl Peroxy Radicals, *J. Phys. Chem.*
762 *A*, 121, 1470-1479, 10.1021/acs.jpca.6b12787, 2017.

763 Krechmer, J. E., Coggon, M. M., Massoli, P., Nguyen, T. B., Crouse, J. D., Hu, W. W., Day, D. A.,
764 Tyndall, G. S., Henze, D. K., Rivera-Rios, J. C., Nowak, J. B., Kimmel, J. R., Mauldin, R. L., Stark, H.,
765 Jayne, J. T., Sipilä, M., Junninen, H., St Clair, J. M., Zhang, X., Feiner, P. A., Zhang, L., Miller, D. O.,
766 Brune, W. H., Keutsch, F. N., Wennberg, P. O., Seinfeld, J. H., Worsnop, D. R., Jimenez, J. L., and
767 Canagaratna, M. R.: Formation of Low Volatility Organic Compounds and Secondary Organic Aerosol
768 from Isoprene Hydroxyhydroperoxide Low-NO Oxidation, *Environ. Sci. Technol.*, 49, 10330-10339,
769 10.1021/acs.est.5b02031, 2015.

770 Lehtipalo, K., Yan, C., Dada, L., Bianchi, F., Xiao, M., Wagner, R., Stolzenburg, D., Ahonen, L. R.,
771 Amorim, A., Baccarini, A., Bauer, P. S., Baumgartner, B., Bergen, A., Bernhammer, A. K., Breitenlechner,
772 M., Brilke, S., Buchholz, A., Mazon, S. B., Chen, D. X., Chen, X. M., Dias, A., Dommen, J., Draper, D.
773 C., Duplissy, J., Ehn, M., Finkenzeller, H., Fischer, L., Frege, C., Fuchs, C., Garmash, O., Gordon, H.,
774 Hakala, J., He, X. C., Heikkinen, L., Heinritzi, M., Helm, J. C., Hofbauer, V., Hoyle, C. R., Jokinen, T.,
775 Kangasluoma, J., Kerminen, V. M., Kim, C., Kirkby, J., Kontkanen, J., Kürten, A., Lawler, M. J., Mai,
776 H. J., Mathot, S., Mauldin, R. L., Molteni, U., Nichman, L., Nie, W., Nieminen, T., Ojdanic, A., Onnela,
777 A., Passananti, M., Petäjä, T., Piel, F., Pospisilova, V., Quéléver, L. L. J., Rissanen, M. P., Rose, C.,

778 Sarnela, N., Schallhart, S., Schuchmann, S., Sengupta, K., Simon, M., Sipilä, M., Tauber, C., Tomé, A.,
779 Tröstl, J., Väisänen, O., Vogel, A. L., Volkamer, R., Wagner, A. C., Wang, M. Y., Weitz, L., Wimmer, D.,
780 Ye, P. L., Ylisirniö, A., Zha, Q. Z., Carslaw, K. S., Curtius, J., Donahue, N. M., Flagan, R. C., Hansel, A.,
781 Riipinen, I., Virtanen, A., Winkler, P. M., Baltensperger, U., Kulmala, M., and Worsnop, D. R.:
782 Multicomponent new particle formation from sulfuric acid, ammonia, and biogenic vapors, *Science*
783 *Advances*, 4, 10.1126/sciadv.aau5363, 2018.

784 Liu, Y., Nie, W., Qi, X., Li, Y., Xu, T., Liu, C., Ge, D., Chen, L., Niu, G., Wang, J., Yang, L., Wang, L.,
785 Zhu, C., Wang, J., Zhang, Y., Liu, T., Zha, Q., Yan, C., Ye, C., Zhang, G., Hu, R., Huang, R.-J., Chi, X.,
786 Zhu, T., and Ding, A.: The Pivotal Role of Heavy Terpenes and Anthropogenic Interactions in New
787 Particle Formation on the Southeastern Qinghai-Tibet Plateau, *Environ Sci Technol*, 58, 19748-19761,
788 10.1021/acs.est.4c04112, 2024.

789 Liu, Y. L., Liu, C., Nie, W., Li, Y. Y., Ge, D. F., Chen, L. D., Zhu, C. J., Wang, L., Zhang, Y. X., Liu, T.
790 Y., Qi, X. M., Wang, J. P., Huang, D. D., Wang, Z., Yan, C., Chi, X. G., and Ding, A. J.: Exploring
791 condensable organic vapors and their co-occurrence with PM_{2.5} and O₃ in winter in Eastern China,
792 *Environmental Science-Atmospheres*, 3, 282-297, 10.1039/d2ea00143h, 2023.

793 Liu, Y. L., Nie, W., Li, Y. Y., Ge, D. F., Liu, C., Xu, Z. N., Chen, L. D., Wang, T. Y., Wang, L., Sun, P.,
794 Qi, X. M., Wang, J. P., Xu, Z., Yuan, J., Yan, C., Zhang, Y. J., Huang, D. D., Wang, Z., Donahue, N. M.,
795 Worsnop, D., Chi, X. G., Ehn, M., and Ding, A. J.: Formation of condensable organic vapors from
796 anthropogenic and biogenic volatile organic compounds (VOCs) is strongly perturbed by NO_x in eastern
797 China, *Atmospheric Chemistry and Physics*, 21, 14789-14814, 10.5194/acp-21-14789-2021, 2021.

798 McFiggans, G., Mentel, T. F., Wildt, J., Pullinen, I., Kang, S., Kleist, E., Schmitt, S., Springer, M.,
799 Tillmann, R., Wu, C., Zhao, D. F., Hallquist, M., Faxon, C., Le Breton, M., Hallquist, A. M., Simpson,
800 D., Bergstrom, R., Jenkin, M. E., Ehn, M., Thornton, J. A., Alfarra, M. R., Bannan, T. J., Percival, C. J.,
801 Priestley, M., Topping, D., and Kiendler-Scharr, A.: Secondary organic aerosol reduced by mixture of
802 atmospheric vapours, *Nature*, 565, 587-593, 10.1038/s41586-018-0871-y, 2019.

803 Meder, M., Graeffe, F., Luo, Y., Luo, J., Iyer, S., Valiev, R., Cai, R., Rissanen, M., Kurtén, T., Varelas, J.
804 G., Geiger, F. M., Thomson, R. J., and Ehn, M.: Selective Deuteration Reveals the Importance of Multiple
805 Branching Pathways in α -Pinene Autoxidation, *J. Am. Chem. Soc.*, 147, 14131-14138,
806 10.1021/jacs.4c14462, 2025.

807 Moller, K. H., Bates, K. H., and Kjaergaard, H. G.: The Importance of Peroxy Radical Hydrogen-Shift
808 Reactions in Atmospheric Isoprene Oxidation, *J. Phys. Chem. A*, 123, 920-932,
809 10.1021/acs.jpca.8b10432, 2019.

810 Moller, K. H., Otkjær, R. V., Hyttinen, N., Kurtén, T., and Kjaergaard, H. G.: Cost-Effective
811 Implementation of Multiconformer Transition State Theory for Peroxy Radical Hydrogen Shift Reactions,
812 *J. Phys. Chem. A*, 120, 10072-10087, 10.1021/acs.jpca.6b09370, 2016.

813 Murphy, S. E., Crouse, J. D., Poulsen, A. S., Lipson, J. E., Kjaergaard, H. G., and Wennberg, P. O.:
814 Accretion product formation in the self- and cross-reactions of small β -hydroxy peroxy radicals, *Environ.*
815 *Sci. - Atmospheres*, 5, 1312-1325, 10.1039/d5ea00106d, 2025.

816 Ng, N. L., Kwan, A. J., Surratt, J. D., Chan, A. W. H., Chhabra, P. S., Sorooshian, A., Pye, H. O. T.,
817 Crouse, J. D., Wennberg, P. O., Flagan, R. C., and Seinfeld, J. H.: Secondary organic aerosol (SOA)
818 formation from reaction of isoprene with nitrate radicals (NO₃), *Atmos. Chem. Phys.*, 8, 4117-4140,
819 10.5194/acp-8-4117-2008, 2008.

820 Nguyen, T. B., Coggon, M. M., Bates, K. H., Zhang, X., Schwantes, R. H., Schilling, K. A., Loza, C. L.,
821 Flagan, R. C., Wennberg, P. O., and Seinfeld, J. H.: Organic aerosol formation from the reactive uptake
822 of isoprene epoxydiols (IEPOX) onto non-acidified inorganic seeds, *Atmospheric Chemistry and Physics*,
823 14, 3497-3510, 10.5194/acp-14-3497-2014, 2014.

824 Nguyen, T. B., Bates, K. H., Crounse, J. D., Schwantes, R. H., Zhang, X., Kjaergaard, H. G., Surratt, J.
825 D., Lin, P., Laskin, A., Seinfeld, J. H., and Wennberg, P. O.: Mechanism of the hydroxyl radical oxidation
826 of methacryloyl peroxyxynitrate (MPAN) and its pathway toward secondary organic aerosol formation in
827 the atmosphere, *Phys. Chem. Chem. Phys.*, 17, 17914-17926, 10.1039/c5cp02001h, 2015.

828 Nie, W., Yan, C., Huang, D. D., Wang, Z., Liu, Y., Qiao, X., Guo, Y., Tian, L., Zheng, P., Xu, Z., Li, Y.,
829 Xu, Z., Qi, X., Sun, P., Wang, J., Zheng, F., Li, X., Yin, R., Dallenbach, K. R., Bianchi, F., Petäjä, T.,
830 Zhang, Y., Wang, M., Schervish, M., Wang, S., Qiao, L., Wang, Q., Zhou, M., Wang, H., Yu, C., Yao, D.,
831 Guo, H., Ye, P., Lee, S., Li, Y. J., Liu, Y., Chi, X., Kerminen, V.-M., Ehn, M., Donahue, N. M., Wang, T.,
832 Huang, C., Kulmala, M., Worsnop, D., Jiang, J., and Ding, A.: Secondary organic aerosol formed by
833 condensing anthropogenic vapours over China's megacities, *Nature Geoscience*, 15, 255-261,
834 10.1038/s41561-022-00922-5, 2022.

835 Nie, W., Yan, C., Yang, L., Roldin, P., Liu, Y., Vogel, A. L., Molteni, U., Stolzenburg, D., Finkenzeller,
836 H., Amorim, A., Bianchi, F., Curtius, J., Dada, L., Draper, D. C., Duplissy, J., Hansel, A., He, X.-C.,
837 Hofbauer, V., Jokinen, T., Kim, C., Lehtipalo, K., Niehman, L., Mauldin, R. L., Makhmutov, V., Mentler,
838 B., Mizelli-Ojdanic, A., Petäjä, T., Quéléver, L. L. J., Schallhart, S., Simon, M., Tauber, C., Tomé, A.,
839 Volkamer, R., Wagner, A. C., Wagner, R., Wang, M., Ye, P., Li, H., Huang, W., Qi, X., Lou, S., Liu, T.,
840 Chi, X., Dommen, J., Baltensperger, U., El Haddad, I., Kirkby, J., Worsnop, D., Kulmala, M., Donahue,
841 N. M., Ehn, M., and Ding, A.: NO at low concentration can enhance the formation of highly oxygenated
842 biogenic molecules in the atmosphere, *Nat. Commun.*, 14, 3347, 10.1038/s41467-023-39066-4, 2023.

843 Otkjaer, R. V., Jakobsen, H. H., Tram, C. M., and Kjaergaard, H. G.: Calculated Hydrogen Shift Rate
844 Constants in Substituted Alkyl Peroxy Radicals, *J. Phys. Chem. A*, 122, 8665-8673,
845 10.1021/acs.jpca.8b06223, 2018.

846 Paulot, F., Crounse, J. D., Kjaergaard, H. G., Kürten, A., St Clair, J. M., Seinfeld, J. H., and Wennberg,
847 P. O.: Unexpected Epoxide Formation in the Gas-Phase Photooxidation of Isoprene, *Science*, 325, 730-
848 733, 10.1126/science.1172910, 2009.

849 Peräkylä, O., Berndt, T., Franzon, L., Hasan, G., Meder, M., Valiev, R. R., Daub, C. D., Varelas, J. G.,
850 Geiger, F. M., Thomson, R. J., Rissanen, M., Kurtén, T., and Ehn, M.: Large Gas-Phase Source of Esters
851 and Other Accretion Products in the Atmosphere, *J. Am. Chem. Soc.*, 145, 7780-7790,
852 10.1021/jacs.2c10398, 2023.

853 Praske, E., Otkjaer, R. V., Crounse, J. D., Hethcox, J. C., Stoltz, B. M., Kjaergaard, H. G., and Wennberg,
854 P. O.: Atmospheric autoxidation is increasingly important in urban and suburban North America, *Proc.*
855 *Natl. Acad. Sci. U. S. A.*, 115, 64-69, 10.1073/pnas.1715540115, 2018.

856 Riccobono, F., Schobesberger, S., Scott, C. E., Dommen, J., Ortega, I. K., Rondo, L., Almeida, J.,
857 Amorim, A., Bianchi, F., Breitenlechner, M., David, A., Downard, A., Dunne, E. M., Duplissy, J., Ehrhart,
858 S., Flagan, R. C., Franchin, A., Hansel, A., Junninen, H., Kajos, M., Keskinen, H., Kupc, A., Kurten, A.,
859 Kvashin, A. N., Laaksonen, A., Lehtipalo, K., Makhmutov, V., Mathot, S., Nieminen, T., Onnela, A.,
860 Petaja, T., Praplan, A. P., Santos, F. D., Schallhart, S., Seinfeld, J. H., Sipila, M., Spracklen, D. V.,
861 Stozhkov, Y., Stratmann, F., Tome, A., Tsagkogeorgas, G., Vaattovaara, P., Viisanen, Y., Vrtala, A.,
862 Wagner, P. E., Weingartner, E., Wex, H., Wimmer, D., Carslaw, K. S., Curtius, J., Donahue, N. M., Kirkby,

863 J., Kulmala, M., Worsnop, D. R., and Baltensperger, U.: Oxidation Products of Biogenic Emissions
864 Contribute to Nucleation of Atmospheric Particles, *Science*, 344, 717-721, 10.1126/science.1243527,
865 2014.

866 Richters, S., Herrmann, H., and Berndt, T.: Highly Oxidized RO₂ Radicals and Consecutive Products
867 from the Ozonolysis of Three Sesquiterpenes, *Environ. Sci. Technol.*, 50, 2354-2362,
868 10.1021/acs.est.5b05321, 2016a.

869 Richters, S., Herrmann, H., and Berndt, T.: Different pathways of the formation of highly oxidized
870 multifunctional organic compounds (HOMs) from the gas-phase ozonolysis of β -caryophyllene,
871 *Atmospheric Chemistry and Physics*, 16, 9831-9845, 10.5194/acp-16-9831-2016, 2016b.

872 Riva, M., Rantala, P., Krechmer, J. E., Peräkylä, O., Zhang, Y. J., Heikkinen, L., Garmash, O., Yan, C.,
873 Kulmala, M., Worsnop, D., and Ehn, M.: Evaluating the performance of five different chemical ionization
874 techniques for detecting gaseous oxygenated organic species, *Atmos. Meas. Tech.*, 12, 2403-2421,
875 10.5194/amt-12-2403-2019, 2019.

876 Roldin, P., Eriksson, A. C., Nordin, E. Z., Hermansson, E., Mogensen, D., Rusanen, A., Boy, M.,
877 Swietlicki, E., Svenningsson, B., Zelenyuk, A., and Pagels, J.: Modelling non-equilibrium secondary
878 organic aerosol formation and evaporation with the aerosol dynamics, gas- and particle-phase chemistry
879 kinetic multilayer model ADCHAM, *Atmospheric Chemistry and Physics*, 14, 7953-7993, 10.5194/acp-
880 14-7953-2014, 2014.

881 Roldin, P., Ehn, M., Kurtén, T., Olenius, T., Rissanen, M. P., Sarnela, N., Elm, J., Rantala, P., Hao, L.,
882 Hyttinen, N., Heikkinen, L., Worsnop, D. R., Pichelstorfer, L., Xavier, C., Clusius, P., Öström, E., Petäjä,
883 T., Kulmala, M., Vehkamäki, H., Virtanen, A., Riipinen, I., and Boy, M.: The role of highly oxygenated
884 organic molecules in the Boreal aerosol-cloud-climate system, *Nat. Commun.*, 10, 4370,
885 10.1038/s41467-019-12338-8, 2019.

886 Schervish, M. and Donahue, N. M.: Peroxy radical chemistry and the volatility basis set, *Atmospheric*
887 *Chemistry and Physics*, 20, 1183-1199, 10.5194/acp-20-1183-2020, 2020.

888 Schervish, M., Heinritzi, M., Stolzenburg, D., Dada, L., Wang, M. Y., Ye, Q., Hofbauer, V., Devivo, J.,
889 Bianchi, F., Brilke, S., Duplissy, J., El Haddad, I., Finkenzeller, H., He, X. C., Kuvshinov, A., Kim, C.,
890 Kirkby, J., Kulmala, M., Lehtipalo, K., Lopez, B., Makhmutov, V., Mentler, B., Molteni, U., Nie, W.,
891 Petäjä, T., Quéléver, L., Volkamer, R., Wagner, A. C., Winkler, P., Yan, C., and Donahue, N. M.:
892 Interactions of peroxy radicals from monoterpene and isoprene oxidation simulated in the radical
893 volatility basis set, *Environmental Science-Atmospheres*, 4, 740-753, 10.1039/d4ea00056k, 2024.

894 Shen, H. R., Vereecken, L., Kang, S. A., Pullinen, I., Fuchs, H., Zhao, D. F., and Mentel, T. F.: Unexpected
895 significance of a minor reaction pathway in daytime formation of biogenic highly oxygenated organic
896 compounds, *Science Advances*, 8, 10.1126/sciadv.abp8702, 2022.

897 Shen, J. L., Russell, D. M., Devivo, J., Kunkler, F., Baalbaki, R., Mentler, B., Scholz, W., Yu, W. J.,
898 Caudillo-Plath, L., Sommer, E., Ahongshangbam, E., Alfaouri, D., Almeida, J., Amorim, A., Beck, L. J.,
899 Beckmann, H., Berntheusel, M., Bhattacharyya, N., Canagaratna, M. R., Chassaing, A., Cruz-Simbron,
900 R., Dada, L., Duplissy, J., Gordon, H., Granzin, M., Schute, L. G., Heinritzi, M., Iyer, S., Klebach, H.,
901 Krueger, T., Kuerten, A., Lampimäki, M., Liu, L., Lopez, B., Martinez, M., Morawiec, A., Onnela, A.,
902 Peltola, M., Rato, P., Reza, M., Richter, S., Roerup, B., Sebastian, M. K., Simon, M., Surdu, M., Tamme,
903 K., Thakur, R. C., Tome, A., Tong, Y. D., Top, J., Umo, N. S., Unfer, G., Vettikkat, L., Weissbacher, J.,
904 Xenofontos, C., Yang, B. X., Zauner-Wieczorek, M., Zhang, J. Y., Zheng, Z. S., Baltensperger, U.,

905 Christoudias, T., Flagan, R. C., El Haddad, I., Junninen, H., Moehler, O., Riipinen, I., Rohner, U.,
906 Schobesberger, S., Volkamer, R., Winkler, P. M., Hansel, A., Lehtipalo, K., Donahue, N. M., Lelieveld,
907 J., Harder, H., Kulmala, M., Worsnop, D. R., Kirkby, J., Curtius, J., and He, X. C.: New particle formation
908 from isoprene under upper-tropospheric conditions, *Nature*, 636, 10.1038/s41586-024-08196-0, 2024.

909 Simon, M., Dada, L., Heinritzi, M., Scholz, W., Stolzenburg, D., Fischer, L., Wagner, A. C., Kurten, A.,
910 Rorup, B., He, X. C., Almeida, J., Baalbaki, R., Baccharini, A., Bauer, P. S., Beck, L., Bergen, A., Bianchi,
911 F., Brakling, S., Brilke, S., Caudillo, L., Chen, D. X., Chu, B. W., Dias, A., Draper, D. C., Duplissy, J.,
912 El-Haddad, I., Finkenzeller, H., Frege, C., Gonzalez-Carracedo, L., Gordon, H., Granzin, M., Hakala, J.,
913 Hofbauer, V., Hoyle, C. R., Kim, C., Kong, W. M., Lamkaddam, H., Lee, C. P., Lehtipalo, K., Leiminger,
914 M., Mai, H. J., Manninen, H. E., Marie, G., Marten, R., Mentler, B., Molteni, U., Nichman, L., Nie, W.,
915 Ojdanic, A., Onnela, A., Partoll, E., Petaja, T., Pfeifer, J., Philippov, M., Quelever, L. L. J., Ranjithkumar,
916 A., Rissanen, M. P., Schallhart, S., Schobesberger, S., Schuchmann, S., Shen, J. L., Sipila, M., Steiner,
917 G., Stozhkov, Y., Tauber, C., Tham, Y. J., Tome, A. R., Vazquez-Pufleau, M., Vogel, A. L., Wagner, R.,
918 Wang, M. Y., Wang, D. S., Wang, Y. H., Weber, S. K., Wu, Y. S., Xiao, M., Yan, C., Ye, P. L., Ye, Q.,
919 Zauner-Wieczorek, M., Zhou, X. Q., Baltensperger, U., Dommen, J., Flagan, R. C., Hansel, A., Kulmala,
920 M., Volkamer, R., Winkler, P. M., Worsnop, D. R., Donahue, N. M., Kirkby, J., and Curtius, J.: Molecular
921 understanding of new-particle formation from alpha-pinene between -50 and +25 °C, *Atmospheric
922 Chemistry and Physics*, 20, 9183-9207, 10.5194/acp-20-9183-2020, 2020.

923 Sindelarova, K., Granier, C., Bouarar, I., Guenther, A., Tilmes, S., Stavrou, T., Müller, J. F., Kuhn, U.,
924 Stefani, P., and Knorr, W.: Global data set of biogenic VOC emissions calculated by the MEGAN model
925 over the last 30 years, *Atmospheric Chemistry and Physics*, 14, 9317-9341, 10.5194/acp-14-9317-2014,
926 2014.

927 Stolzenburg, D., Fischer, L., Vogel, A. L., Heinritzi, M., Schervish, M., Simon, M., Wagner, A. C., Dada,
928 L., Ahonen, L. R., Amorim, A., Baccharini, A., Bauer, P. S., Baumgartner, B., Bergen, A., Bianchi, F.,
929 Breitenlechner, M., Brilke, S., Mazon, S. B., Chen, D. X., Dias, A., Draper, D. C., Duplissy, J., Haddad,
930 I., Finkenzeller, H., Frege, C., Fuchs, C., Garmash, O., Gordon, H., He, X., Helm, J., Hofbauer, V., Hoyle,
931 C. R., Kim, C., Kirkby, J., Kontkanen, J., Kuerten, A., Lampilahti, J., Lawler, M., Lehtipalo, K.,
932 Leiminger, M., Mai, H., Mathot, S., Mentler, B., Molteni, U., Nie, W., Nieminen, T., Nowak, J. B.,
933 Ojdanic, A., Onnela, A., Passananti, M., Petaja, T., Quelever, L. L. J., Rissanen, M. P., Sarnela, N.,
934 Schallhart, S., Tauber, C., Tome, A., Wagner, R., Wang, M., Weitz, L., Wimmer, D., Xiao, M., Yan, C.,
935 Ye, P., Zha, Q., Baltensperger, U., Curtius, J., Dommen, J., Flagan, R. C., Kulmala, M., Smith, J. N.,
936 Worsnop, D. R., Hansel, A., Donahue, N. M., and Winkler, P. M.: Rapid growth of organic aerosol
937 nanoparticles over a wide tropospheric temperature range, *Proc. Natl. Acad. Sci. U. S. A.*, 115, 9122-
938 9127, 10.1073/pnas.1807604115, 2018.

939 Sun, H., Liu, Y., Nie, W., Li, Y., Ge, D., Xu, T., Yin, J., Liu, C., Fu, Z., Qi, X., Liu, T., Zha, Q., Yan, C.,
940 Wang, Z., Chi, X., and Ding, A.: Unexpected Gas-Phase Formation of Glycolic Acid Sulfate in the
941 Atmosphere, *Environ Sci Technol*, 59, 16556-16566, 10.1021/acs.est.5c07888, 2025.

942 Trostl, J., Chuang, W. K., Gordon, H., Heinritzi, M., Yan, C., Molteni, U., Ahlm, L., Frege, C., Bianchi,
943 F., Wagner, R., Simon, M., Lehtipalo, K., Williamson, C., Craven, J. S., Duplissy, J., Adamov, A.,
944 Almeida, J., Bernhammer, A. K., Breitenlechner, M., Brilke, S., Dias, A., Ehrhart, S., Flagan, R. C.,
945 Franchin, A., Fuchs, C., Guida, R., Gysel, M., Hansel, A., Hoyle, C. R., Jokinen, T., Junninen, H.,
946 Kangasluoma, J., Keskinen, H., Kim, J., Krapf, M., Kurten, A., Laaksonen, A., Lawler, M., Leiminger,
947 M., Mathot, S., Mohler, O., Nieminen, T., Onnela, A., Petaja, T., Piel, F. M., Miettinen, P., Rissanen, M.

948 P., Rondo, L., Sarnela, N., Schobesberger, S., Sengupta, K., Sipila, M., Smith, J. N., Steiner, G., Tome,
949 A., Virtanen, A., Wagner, A. C., Weingartner, E., Wimmer, D., Winkler, P. M., Ye, P. L., Carslaw, K. S.,
950 Curtius, J., Dommen, J., Kirkby, J., Kulmala, M., Riipinen, I., Worsnop, D. R., Donahue, N. M., and
951 Baltensperger, U.: The role of low-volatility organic compounds in initial particle growth in the
952 atmosphere, *Nature*, 533, 527-531, 10.1038/nature18271, 2016.

953 Wang, S. N., Riva, M., Yan, C., Ehn, M., and Wang, L. M.: Primary Formation of Highly Oxidized
954 Multifunctional Products in the OH-Initiated Oxidation of Isoprene: A Combined Theoretical and
955 Experimental Study, *Environ. Sci. Technol.*, 52, 12255-12264, 10.1021/acs.est.8b02783, 2018.

956 Weber, J., Archer-Nicholls, S., Griffiths, P., Berndt, T., Jenkin, M., Gordon, H., Knote, C., and Archibald,
957 A. T.: CRI-HOM: A novel chemical mechanism for simulating highly oxygenated organic molecules
958 (HOMs) in global chemistry-aerosol-climate models, *Atmospheric Chemistry and Physics*, 20, 10889-
959 10910, 10.5194/acp-20-10889-2020, 2020.

960 Wennberg, P. O., Bates, K. H., Crounse, J. D., Dodson, L. G., McVay, R. C., Mertens, L. A., Nguyen, T.
961 B., Praske, E., Schwantes, R. H., Smarte, M. D., St Clair, J. M., Teng, A. P., Zhang, X., and Seinfeld, J.
962 H.: Gas-Phase Reactions of Isoprene and Its Major Oxidation Products, *Chem. Rev.*, 118, 3337-3390,
963 10.1021/acs.chemrev.7b00439, 2018.

964 Xu, Z. N., Nie, W., Liu, Y. L., Sun, P., Huang, D. D., Yan, C., Krechmer, J., Ye, P. L., Xu, Z., Qi, X. M.,
965 Zhu, C. J., Li, Y. Y., Wang, T. Y., Wang, L., Huang, X., Tang, R. Z., Guo, S., Xiu, G. L., Fu, Q. Y.,
966 Worsnop, D., Chi, X. G., and Ding, A. J.: Multifunctional Products of Isoprene Oxidation in Polluted
967 Atmosphere and Their Contribution to SOA, *Geophysical Research Letters*, 48, 10.1029/2020gl089276,
968 2021.

969 Yang, H., Raucci, U., Iyer, S., Hasan, G., Almeida, T. G., Barua, S., Savolainen, A., Kangasluoma, J.,
970 Rissanen, M., Vehkamäki, H., and Kurtén, T.: Molecular dynamics-guided reaction discovery reveals
971 endoperoxide-to-alkoxy radical isomerization as key branching point in α -pinene ozonolysis, *Nat.*
972 *Commun.*, 16, 12, 10.1038/s41467-025-55985-w, 2025a.

973 Yang, L., Nie, W., Yan, C., Ehn, M., Liu, Y., Roldin, P., Qi, X., Kerminen, V.-M., Donahue, N. M.,
974 Worsnop, D., Kulmala, M., and Ding, A.: A mechanistic understanding of the varying yields of highly
975 oxygenated organic molecules, *Nature Communications*, 17, 302, 10.1038/s41467-025-67007-w, 2025b.

976 Zha, Q. Z., Aliaga, D., Krejci, R., Sinclair, V. A., Wu, C., Ciarelli, G., Scholz, W., Heikkinen, L., Partoll,
977 E., Gramlich, Y., Huang, W., Leiminger, M., Enroth, J., Peräkylä, O., Cai, R. L., Chen, X. M., Koenig,
978 A. M., Velarde, F., Moreno, I., Petäjä, T., Artaxo, P., Laj, P., Hansel, A., Carbone, S., Kulmala, M.,
979 Andrade, M., Worsnop, D., Mohr, C., and Bianchi, F.: Oxidized organic molecules in the tropical free
980 troposphere over Amazonia, *Natl. Sci. Rev.*, 11, 11, 10.1093/nsr/nwad138, 2024.

981 Zhao, D. F., Pullinen, I., Fuchs, H., Schrade, S., Wu, R. R., Acir, I. H., Tillmann, R., Rohrer, F., Wildt, J.,
982 Guo, Y. D., Kiendler-Scharr, A., Wahner, A., Kang, S., Vereecken, L., and Mentel, T. F.: Highly
983 oxygenated organic molecule (HOM) formation in the isoprene oxidation by NO_3 radical, *Atmospheric*
984 *Chemistry and Physics*, 21, 9681-9704, 10.5194/acp-21-9681-2021, 2021.

985